DASA 1357 (III)

UNDERGROUND EFFECTS OF NUCLEAR WEAPONS IN THE CLOSE-IN REGION

G. F. McDonough, Jr.

FINAL REPORT

Contract No. DA-49-146-XZ-073

15 March 1963

Volume III of IV Volumes

Engineering Division
E. H. PLESSET ASSOCIATES, INC.
Santa Monica, California

Prepared for

Headquarters
Defense Atomic Support Agency
Washington 25, D. C.
Task No. 13.092

DASA 1357 (III)

UNDERGROUND EFFECTS OF NUCLEAR WEAPONS IN THE CLOSE-IN REGION

G. F. McDonough, Jr.

FINAL REPORT

Contract No. DA-49-146-XZ-073

15 March 1963

Volume III of IV Volumes

Engineering Division
E. H. PLESSET ASSOCIATES, INC.
Santa Monica, California

Prepared for

Headquarters
Defense Atomic Support Agency
Washington 25, D. C.
Task No. 13.092

TABLE OF CONTENTS

CHAPTER VII

SUMMARY OF FREE FIELD EFFECTS

This brief resume of free field effects is based entirely on the data described and presented in Volumes I, II, and IV. The discussion is given in two parts: air-induced effects and directly-transmitted effects. No means of combining air-induced and directly-transmitted effects has been developed as yet; therefore, only surmise is possible regarding the possible combination of these effects. This part of the description of close-in weapons effects will remain unknown until a study of this aspect of the problem has been made. Such work has been proposed and results are to be expected within a year.

Rayleigh wave effects are not included in this description of air-induced effects; the elimination of these effects is based on conclusions drawn from the studies of Gilbert and others described in Volumes I and IV. Simplifications involved in the Rayleigh wave analysis limit these conclusions; however, they are sufficient to define the relative importance of the Rayleigh wave contribution, at least with regard to stresses, because the solution overestimates these effects. These conclusions are as follows: 1.) The Rayleigh wave is never of primary importance for horizontal stresses in the superseismic case; therefore, only materials having seismic velocities greater than 8,300 ft/sec (the air-blast wave velocity at P_{so} = 1,000 psi) will exhibit important Rayleigh wave effects in the close-in region. 2.) The Rayleigh wave is never of great importance for vertical stresses at any location for any material. 3.) The Rayleigh wave horizontal stresses are opposite in sign to those accompanying the air blast wave and tend to reduce the effects of the latter; for vertical stresses the results generally are additive but the Rayleigh wave contribution is of minor importance. 4.) When Rayleigh wave effects are important the stresses involved are tensile.

Based on the above conclusions, stresses arising from the Rayleigh wave appear to be of less importance than are other air-induced effects in the close-in region and can be neglected for most design applications without introducing appreciable error into the analysis. In order to make a comparable statement regarding ground motions, it will be necessary to base any future analysis on a more realistic representation of the air blast pulse.

A. AIR-INDUCED PHENOMENA

Comparison of the AMF and SRI data shows close agreement in all cases except horizontal displacements. Of course, there is an additional difference in that the AMF solution is incapable of providing information concerning tangential stresses, etc., because of the basic assumption of a plane shock front. Furthermore, for the two lower seismic velocities (i.e., c_p = 2,000, 6,000 ft/sec), the SRI results show that radial and tangential stresses are approximately equal. For c_p = 12,000 ft/sec, tangential stresses are as much as 20 percent lower than radial stresses; this is not considered a significant difference for most design applications.

Time plots of vertical and horizontal stress at any depth, assuming that tangential stress equals radial stress and describing both as horizontal stress, can be drawn from the curves for surface stress. The times of transit to any depth can be determined by dividing the depth by c_p and c_s. The attenuation of peak stress with depth can be neglected without serious error, particularly for higher overpressures and lower seismic velocities. The largest attenuation shown by the AMF data is about 30 percent in 80 feet for P_{so} = 1,000 psi and c_p = 6,000 ft/sec., and for P_{so} = 5,000 psi and c_p = 12,000 ft/sec. The SRI data for these cases, although somewhat more irregular than the AMF data, indicate only about 10 percent attenuation on the average. If the surface pressure pulse is used as the stress history below the surface, a correction should be made for the shear discontinuity. At the surface, of course, the dilatational and shear disturbances arrive simultaneously at time, t_o. The shear effect adds to the vertical stress at the surface (as it increases this stress at depths) and reduces by an equal amount the horizontal stress (as it decreases this stress at depths). The amount of the shear discontinuity is much more dependent on seismic velocity than on overpressure

level; for c_p = 2,000 ft/sec the jump can be taken as 50 psi, for c_p = 6,000 ft/sec it is 250 psi, and for c_p = 12,000 ft/sec it is 1,000 psi. In using this method to draw stress curves, the vertical peak stress is the surface peak overpressure, P_{so}. Since horizontal displacements are small at the surface, they may be assumed to be zero. Then horizontal stress, σ_H, is merely $(\nu/1 - \nu)\ P_{so}$ plus the shear jump. For P_{so} = 10,000 psi, c_p = 6,000 ft/sec, ν = 1/3:

$$\sigma_H = \frac{1/3}{2/3}\ (10{,}000) + 250 \text{ psi} = 5{,}250$$

Alternatively, the AMF curves can be interpolated, using the above information as a guide, by establishing decay lines for peak stresses. The surface peak stresses do not lie on this decay line because of the shear jump, as discussed above. Otherwise, curves for all depths have the same smooth shape and the curve for any depth may be sketched in after the peak stress and shear jump have been plotted.

The same techniques can be applied to all other curves in the AMF results. Furthermore, it is possible to interpolate between pressure levels in the same manner (and also to interpolate between pressure levels and depths at the same time) or between seismic velocities. If this means of interpolation leads to confusion, the AMF equations are fairly easy to evaluate for any given situation. Because of the linear nature of the solution, $W^{1/3}$ scaling applies. Also, densities other than 100 lb/ft^3 can be considered by multiplying the response data (stresses are independent of density) by the square root of the ratio of densities (i.e., $\sqrt{100/\gamma}$, where γ is density in lb/ft^3).

Vertical strains can be determined within ± 10 percent for most cases by dividing vertical stress by $\rho\ c_p^2$ where ρ is the density in slugs/ft^3 (for longitudinal waves in bars, Young's modulus, $E = \rho\ c_p^2$). Cases in which the above determination is less accurate are those in which the situation in not strongly superseismic. For these cases (i.e., P_{so} = 5,000 psi, c_p = 12,000 ft/sec; P_{so} = 1,000 psi, c_p = 6,000 ft/sec), the method overestimates strains by as much as 40 percent, but at no time underestimates strains by more than 10 percent. Maximum radial strains given by the SRI data have an approximately constant value of 6×10^{-4} everywhere except at the surface, where they are an order of magnitude less. Tangential stresses increase with depth and are from about 10 to 25 percent of the radial strains.

Vertical displacements show an indefinite increase with time because of the lack of negative phase in the assumed air blast pulse. One means of utilising the data, that of assuming a datum plane of zero displacement and using displacements relative to this level as absolute displacements, has already been discussed. Another simpler method of using the data is by assuming peak displacement to be that occuring when the stress pulse has decayed to some percentage of its peak value. For example, when the stress has decreased to 10 percent of the peak, vertical displacements at a depth of 40 feet for P_{so} = 10,000 psi are 1.2 feet for c_p = 2,000 ft/sec, 0.4 feet for c_p = 6,000 ft/sec, and 0.2 feet for c_p = 12,000 ft/sec. Corresponding values for both P_{so} = 5,000 psi and 1,000 psi are 0.9 feet, 0.3 feet and 0.15 feet.

The SRI data showed larger radial displacements than did the AMF results; however, the time histories had the same shapes and general variation of peak displacement with depth. A simple expression relating maximum radial displacement to surface peak overpressure, seismic velocity, and depth was developed from the SRI results. It is as follows:

$$u_r^* = \left[\frac{0.24\ c_p}{1{,}000} + 2.7\left(\frac{P_{so}}{1{,}000}\right)^{0.17}\right] z^* + 0.01 \qquad (1)$$

Where u_r^* is dimensionless radial displacement and z* is dimensionless depth. The dimensionless depth, z*, is determined from z as follows:

$$z^* = (0.84 \times 10^{-6}\ c_p^{2/3})\ z \qquad (2)$$

and the actual displacement, u_r, is found from u_r^* using:

$$u_r = \frac{15}{\rho c_p^2}\ u_r^* \qquad (3)$$

In all cases, u_θ may be taken as zero without serious error. The maximum error in using Equation (3) to determine u_r is for P_{so} = 988 psi, c_p = 6,000 ft/sec, and z = 18 feet, in which case the displacement is overestimated by 60 percent. For P_{so} = 5,150 psi, c_p = 12,000 ft/sec, and z = 57 feet, the equation underestimates the displacement by 15 percent. Equation (3) is conservative for all but this latter case and gives values always within about 25 percent of those given by the SRI curves.

The above discussion leads to certain conclusions regarding the close-in underground effects. These are as follows:

1. For strongly superseismic situations (i.e., for air blast velocity much greater than ground dilatational velocity) most air-induced ground phenomena can be described fairly well by means of a plane-wave, one-dimensional model. This result agrees well with conclusions based on purely geometric considerations. Lateral stresses are best represented by assuming complete lateral restraint, whereas vertical displacements are more closely determined assuming no lateral restraint although, either assumption leads to reasonably good values of vertical displacement. Thus layering and inelastic effects determined elsewhere using one-dimensional models can be added, at least roughly, to this description of close-in effects.

2. The SRI and AMF data provide, in readily useful form, the necessary inputs to the design of underground structures for air-induced underground effects in the close-in region.

B. DIRECTLY-TRANSMITTED PHENOMENA

The directly-transmitted effects are far less established than are the air-induced effects. The Brode and Bjork hydrodynamic analysis has been applied only to one ground material, Nevada tuff; however, results of Newmark's study indicate that the effect of varying the equation of state within a fairly wide range may not affect results greatly. Since the properties of the Nevada tuff used for the hydrodynamic analysis place it near the borderline of soil and rock, it can be concluded tentatively that the tuff results can be used for other surface materials of interest without great error.

Newmark's results for directly transmitted effects used the hydrodynamic results at a radius of 660 feet as inputs to an elastic solution. Although he demonstrated that the motions and stresses at the boundary of the hydrodynamic and elastic media are little affected by the differences in properties of the two

media, the hydrodynamic analysis results used as inputs were taken at a pressure level below that at which the hydrodynamic assumptions are completely valid. Furthermore, the elastic analysis was begun in a region where elastic behavior is unlikely. Thus the values of stresses and displacements calculated are important more as an indication of decay rates than as design inputs. In fact, the results indicate that stresses and motions are an order of magnitude greater than the air-induced effects at the same ground distance.

The Newmark results require further study to determine the significance of certain features such as the large tensile stresses in the tangential direction, which cannot be sustained by earth materials. The amount of plastic-zone energy attenuation also must be assessed more completely; Brooks' preliminary results indicate this can reduce stresses and motions by more than an order of magnitude. Furthermore, directly-transmitted effects must be evaluated nearer the surface in the range of distances from ground zero which are of prime interest.

Based on the above comments, it must be concluded that further study is required before directly-transmitted effects can be determined analytically in a form suitable for design of near-surface structures in the close-in region. The studies of Newmark and Brooks show great promise of providing this information, but additional effort is necessary in both cases. Until such results are available, reliance must be placed upon the limited field test information which is available. This indicates that most of the directly-transmitted effects at shallow depths occur within 1-1/2 crater radii from the point of burst for a surface detonation. For rock, this corresponds to the distance at which peak surface overpressure, P_{so} = 10,000 psi; for dry soil, P_{so} = 4,000 psi; for wet soil, P_{so} 1,000 psi. Design of near-surface structures can be based on the air-induced ground effects at 10,000 psi (or any lower pressure) for rock or 5,000 psi (or any lower pressure) for dry soil. Locations in wet soil are to be avoided because the crater extends beyond the close-in region.

For all deeply buried structures, directly-transmitted effects predominate. Any analysis or design of such structures must be based on studies such as those of Newmark and Brooks.

C. DESIGN INPUT DATA

Based on the above comments, no quantitative design inputs can be obtained from the Newmark and Brooks descriptions of directly-transmitted effects; however, certain qualitative inputs can be based on these results. These would include the shape of the stress pulses at various locations as well as the variation with location of stresses and displacements. One of the uses to which such results can be put is given in the sample calculations of Chapter IX.

On the basis of the pressure levels associated with crater dimensions in dry soil and rock, design input data should exclude results in soil at pressures $\geq$ 4,000 psi. Then useful results for 10,000 psi are limited to c_p = 12,000 ft/sec and 6,000 ft/sec; for 5,000 psi and below, results for all velocities are applicable.

The most important inputs for most structural designs are the stresses in the medium, particularly the vertical and horizontal stresses. Horizontal and vertical velocities and displacements, as well as shear stresses are of interest but not directly useful in design. Response spectra are useful primarily in designing shock mounts and equipment rather than structures. Curvature of vertical lines can be useful only in determining bending stresses in long, slender, flexible structures. Therefore, the data to be presented here are limited to vertical and horizontal stresses.

Because shallow-buried structures, for which air-induced effects are the most important, are placed by cut-and-cover procedures, there is no possibility of having rock above such a structure in most cases. However, horizontal stresses in rock remain an important design input, particularly for missile silos, which constitute an important class of underground structures.

For the above reasons the data presented here are limited to time histories of stress for the following cases:

P_{so} (psi)	c_p (ft/sec)	Stress Curves Presented
10,000	12,000	σ_H
	6,000	σ_H, σ_z
5,000	12,000	σ_H
	6,000	σ_H, σ_z
	2,000	σ_H, σ_z
1,000	6,000	σ_H, σ_z
	2,000	σ_H, σ_z

These curves are shown in Figures 1 through 12 for depths of 0, 40, 80, and 160 feet. They are essentially the same as the corresponding AMF curves of Appendix C (which are drawn only for 0, 40 and 80 feet) but are drawn to a more convenient scale for design use.

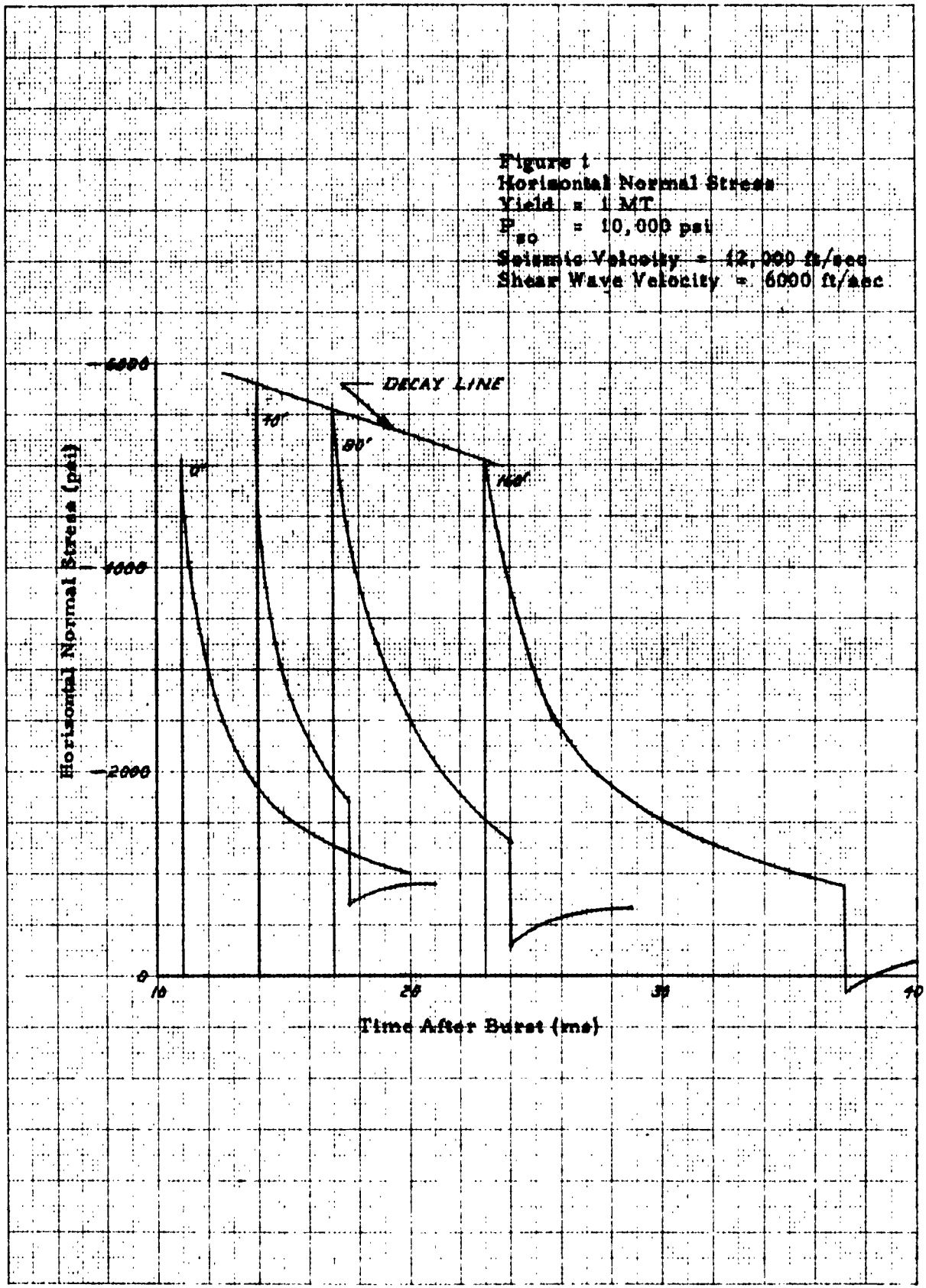
Figure 1
Horizontal Normal Stress
Yield = 1 MT
P_{so} = 10,000 psi
Seismic Velocity = 12,000 ft/sec
Shear Wave Velocity = 6000 ft/sec
DECAY LINE
0°
30°
90°
150°
Horizontal Normal Stress (psi)
6000
4000
2000
0
10
20
30
40
Time After Burst (ms)

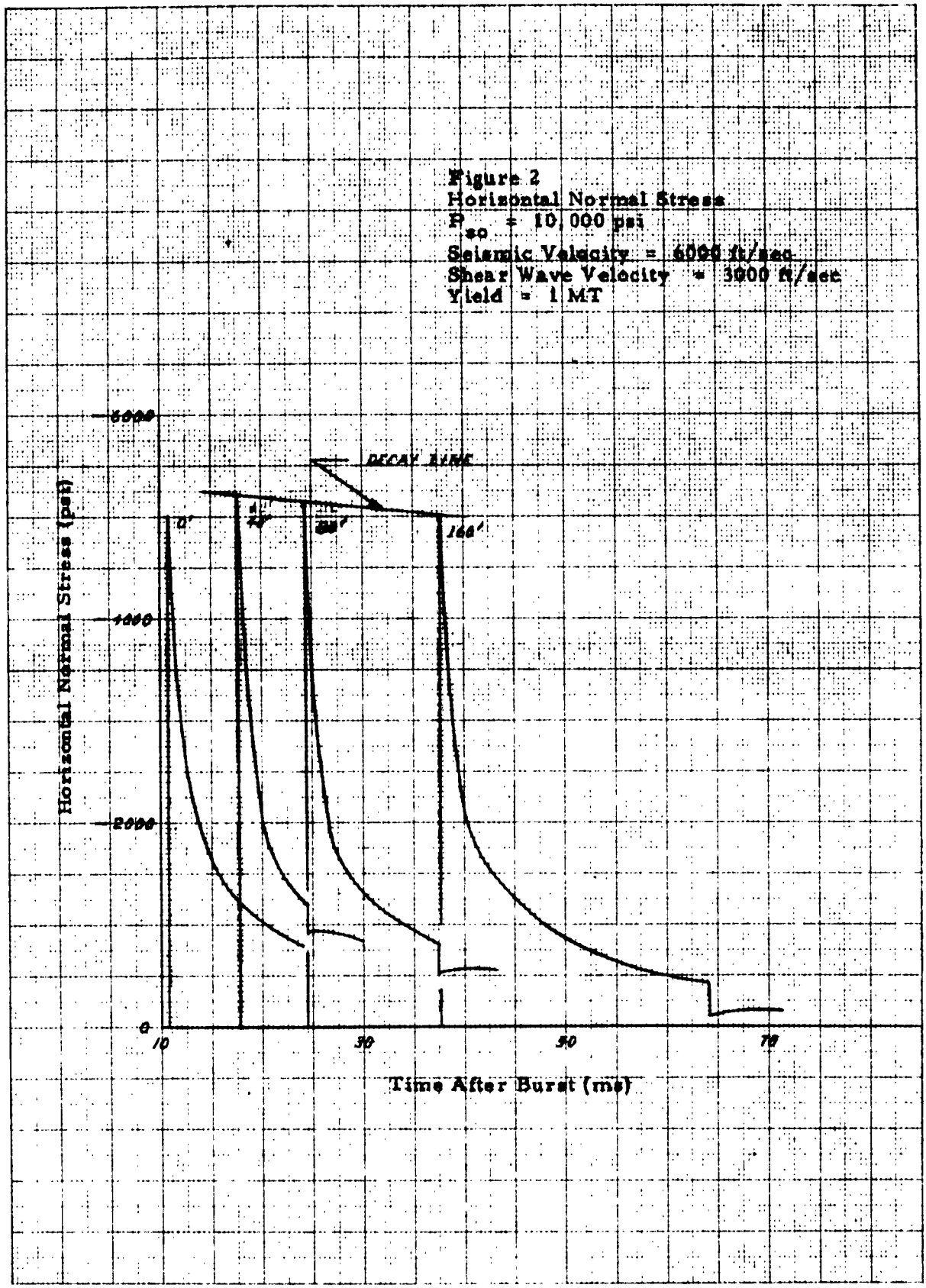
Figure 2
Horizontal Normal Stress
P_{so} = 10,000 psi
Seismic Velocity = 6000 ft/sec
Shear Wave Velocity = 3000 ft/sec
Yield = 1 MT
DECAY TIME
Horizontal Normal Stress (psi)
6000
4000
2000
0
10
30
50
70
Time After Burst (ms)

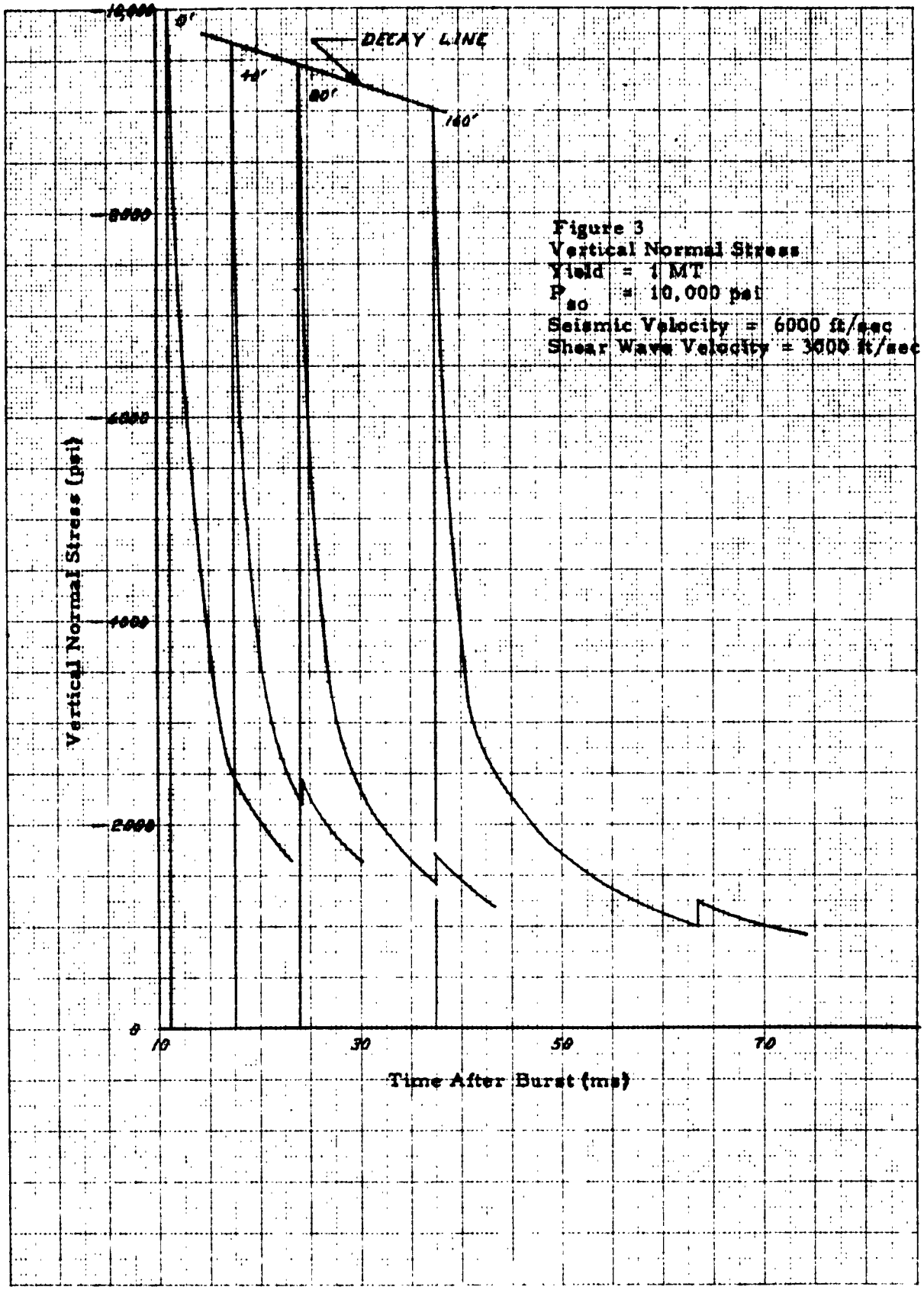

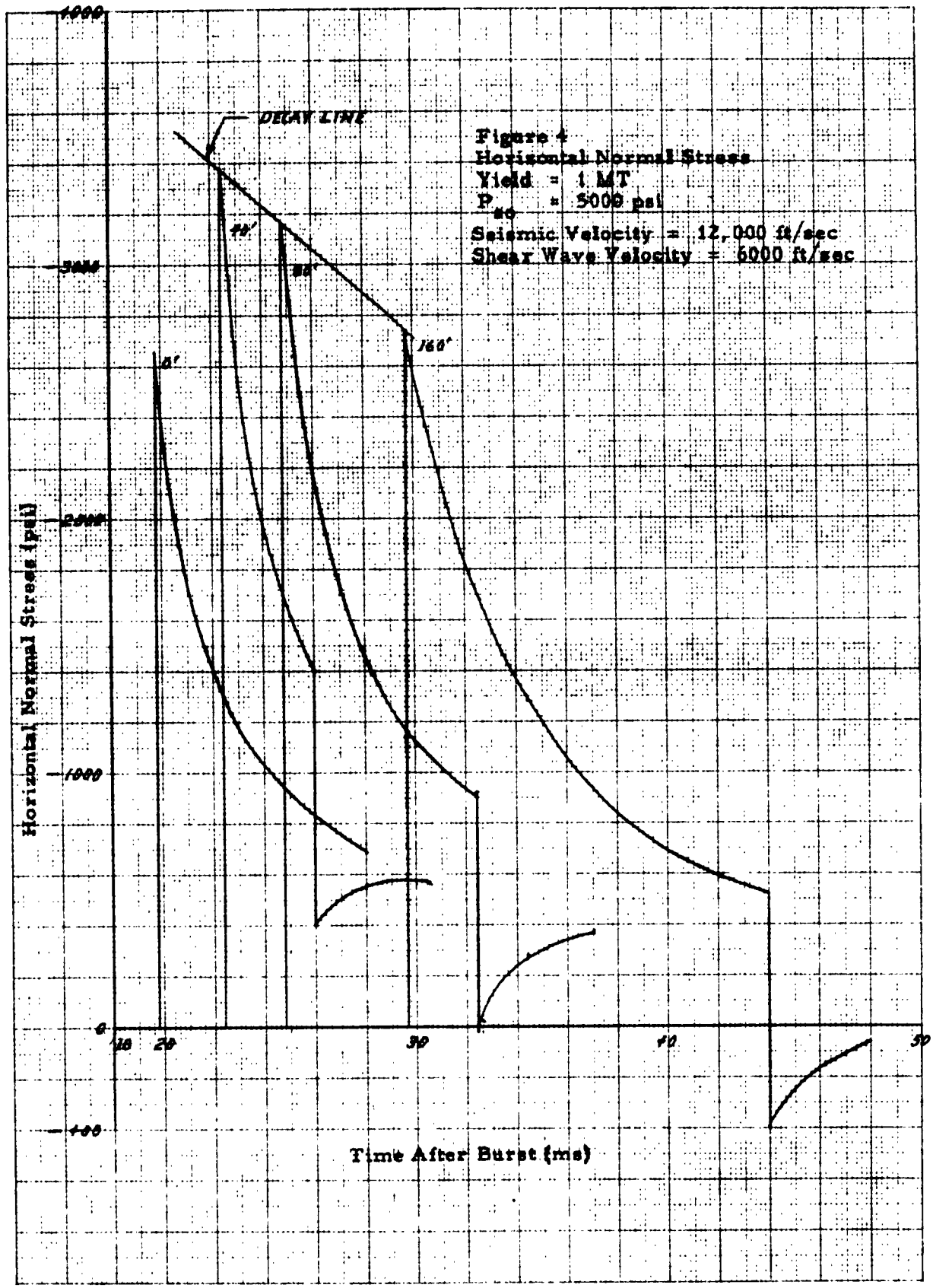
DECAY LINE
Figure 4
Horizontal Normal Stress
Yield = 1 MT
P_{so} = 5000 psi
Seismic Velocity = 12,000 ft/sec
Shear Wave Velocity = 6000 ft/sec
Horizontal Normal Stress (psi)
Time After Burst (ms)
0
1000
2000
3000
4000
-400
10
20
30
40
50
0'
40'
80'
160'

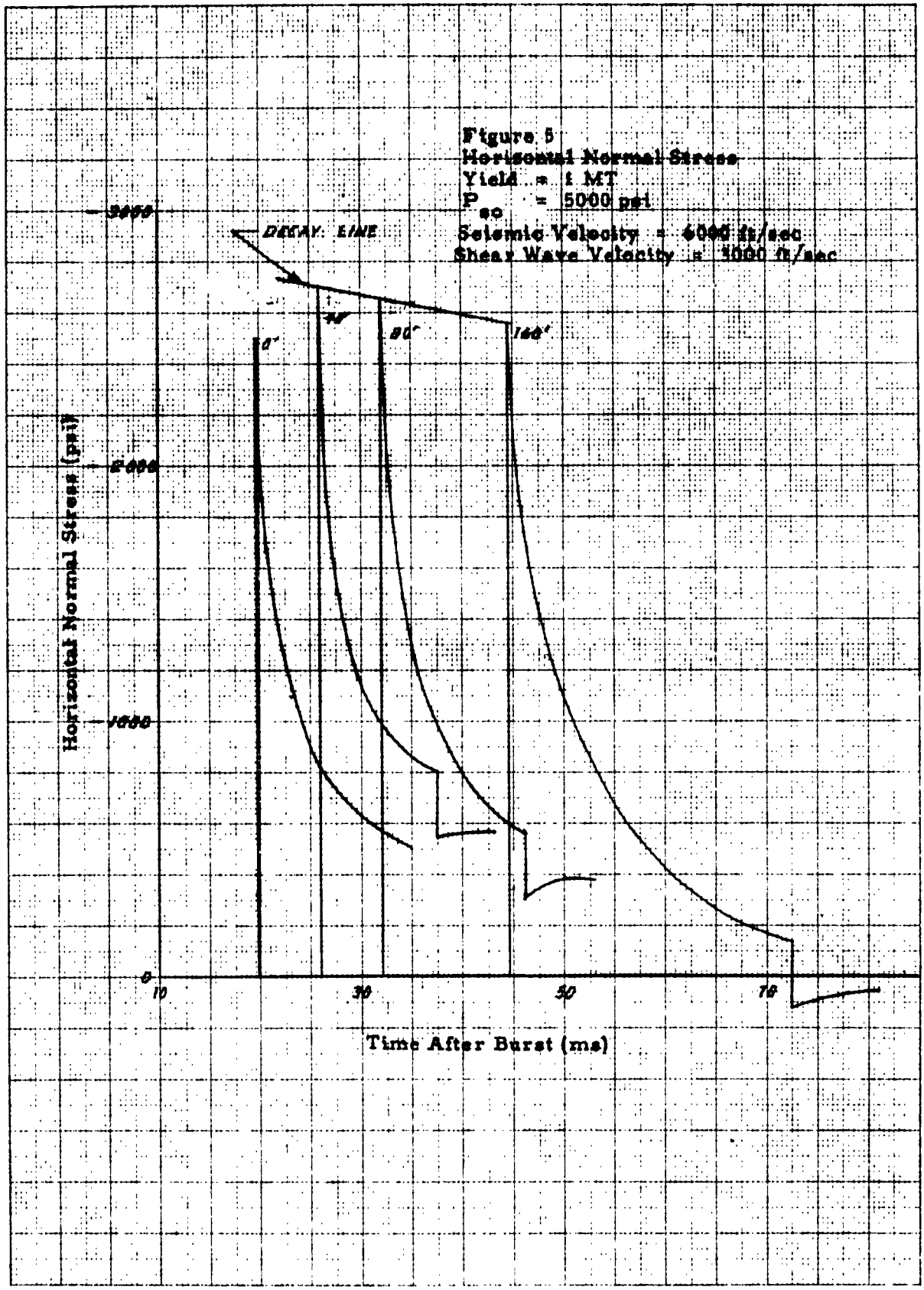
Figure 5
Horizontal Normal Stress
Yield = 1 MT
P so = 5000 psi
Seismic Velocity = 6000 ft/sec
Shear Wave Velocity = 3000 ft/sec
DECAY LINE
0°
30°
90°
180°
Horizontal Normal Stress (psi)
3000
2000
1000
0
10
30
50
70
Time After Burst (ms)

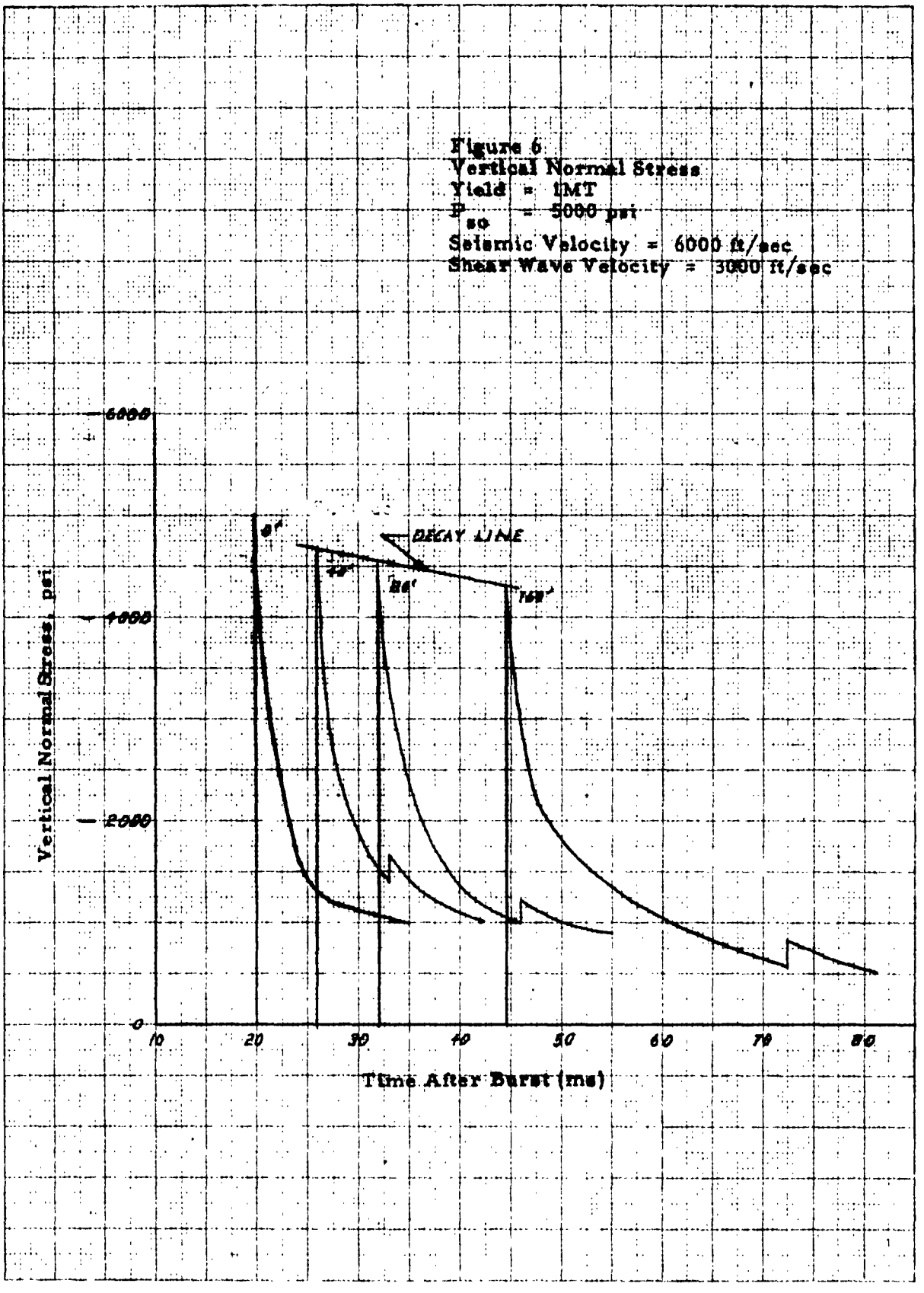

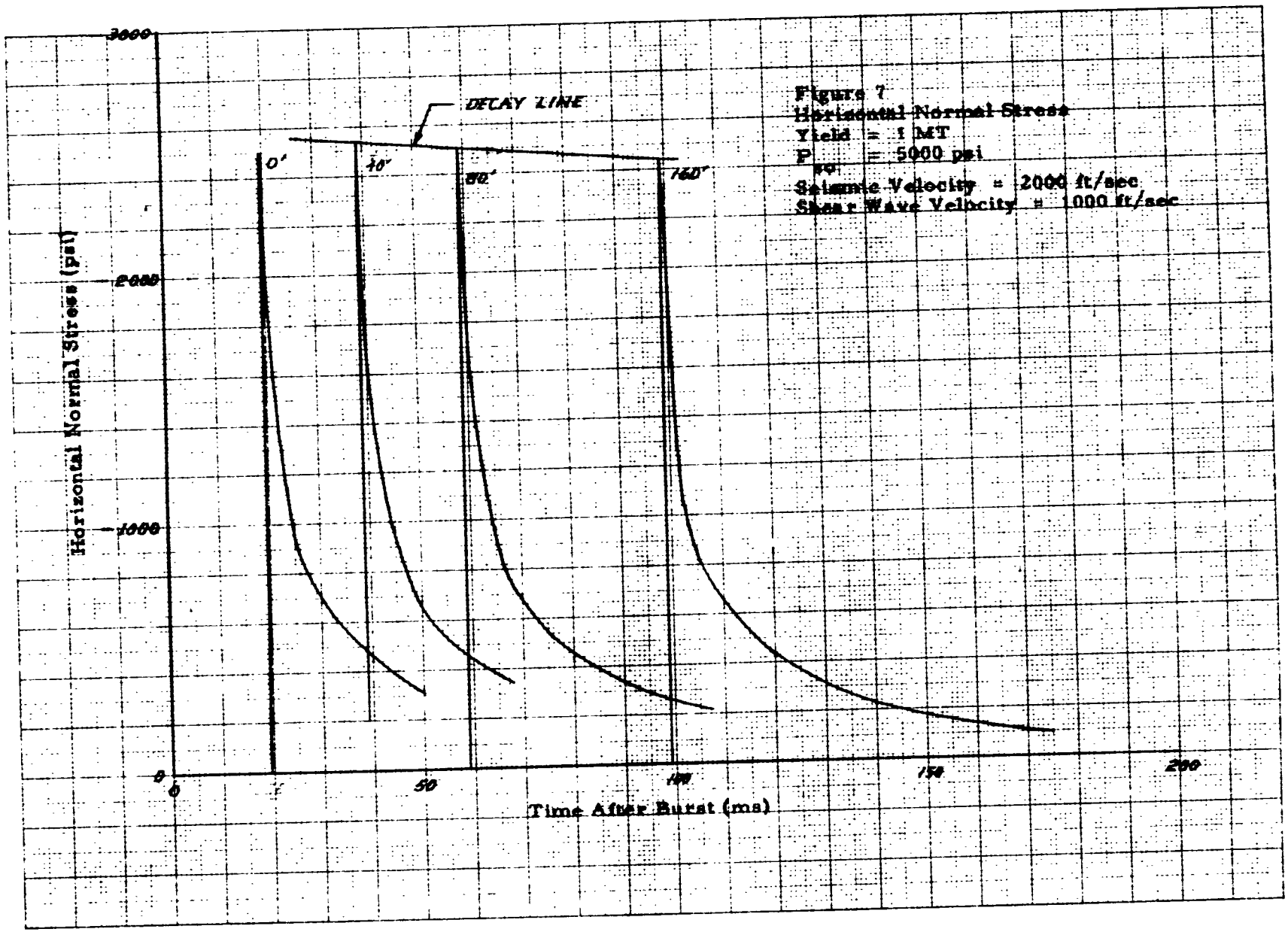

Figure 7
Horizontal Normal Stress
Yield = 1 MT
P_{so} = 5000 psi
Seismic Velocity = 2000 ft/sec
Shear Wave Velocity = 1000 ft/sec

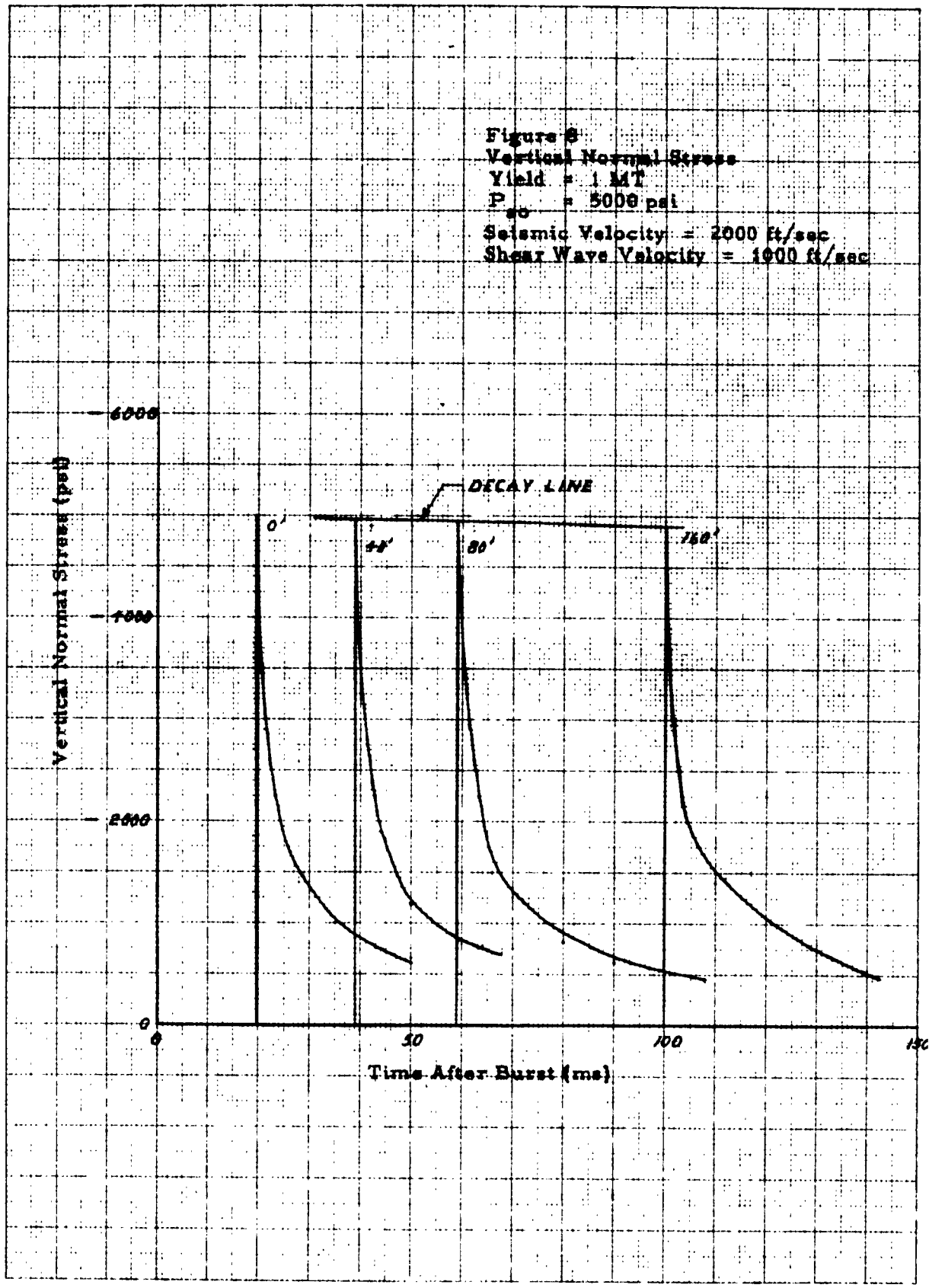
Figure 8
Vertical Normal Stress
Yield = 1 MT
P_{so} = 5000 psi
Seismic Velocity = 2000 ft/sec
Shear Wave Velocity = 1000 ft/sec
Vertical Normal Stress (psi)
6000
4000
2000
0
DECAY LINE
0'
44'
80'
160'
0
50
100
Time After Burst (ms)

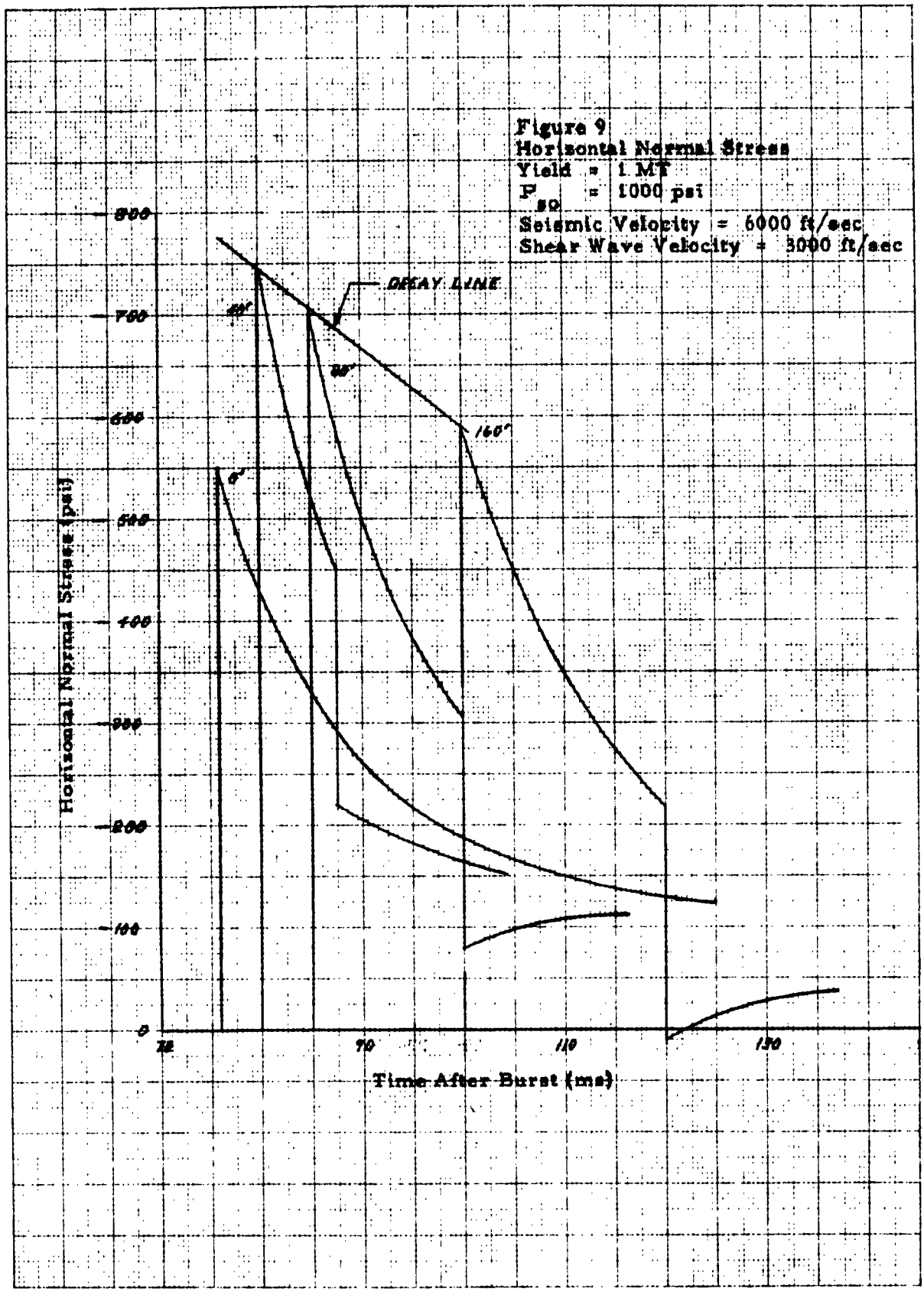
Figure 9
Horizontal Normal Stress
Yield = 1 MT
P_{so} = 1000 psi
Seismic Velocity = 6000 ft/sec
Shear Wave Velocity = 3000 ft/sec
DECAY LINE
40°
80°
160°
0°
Horizontal Normal Stress (psi)
800
700
600
500
400
300
200
100
0
70
110
130
Time After Burst (ms)

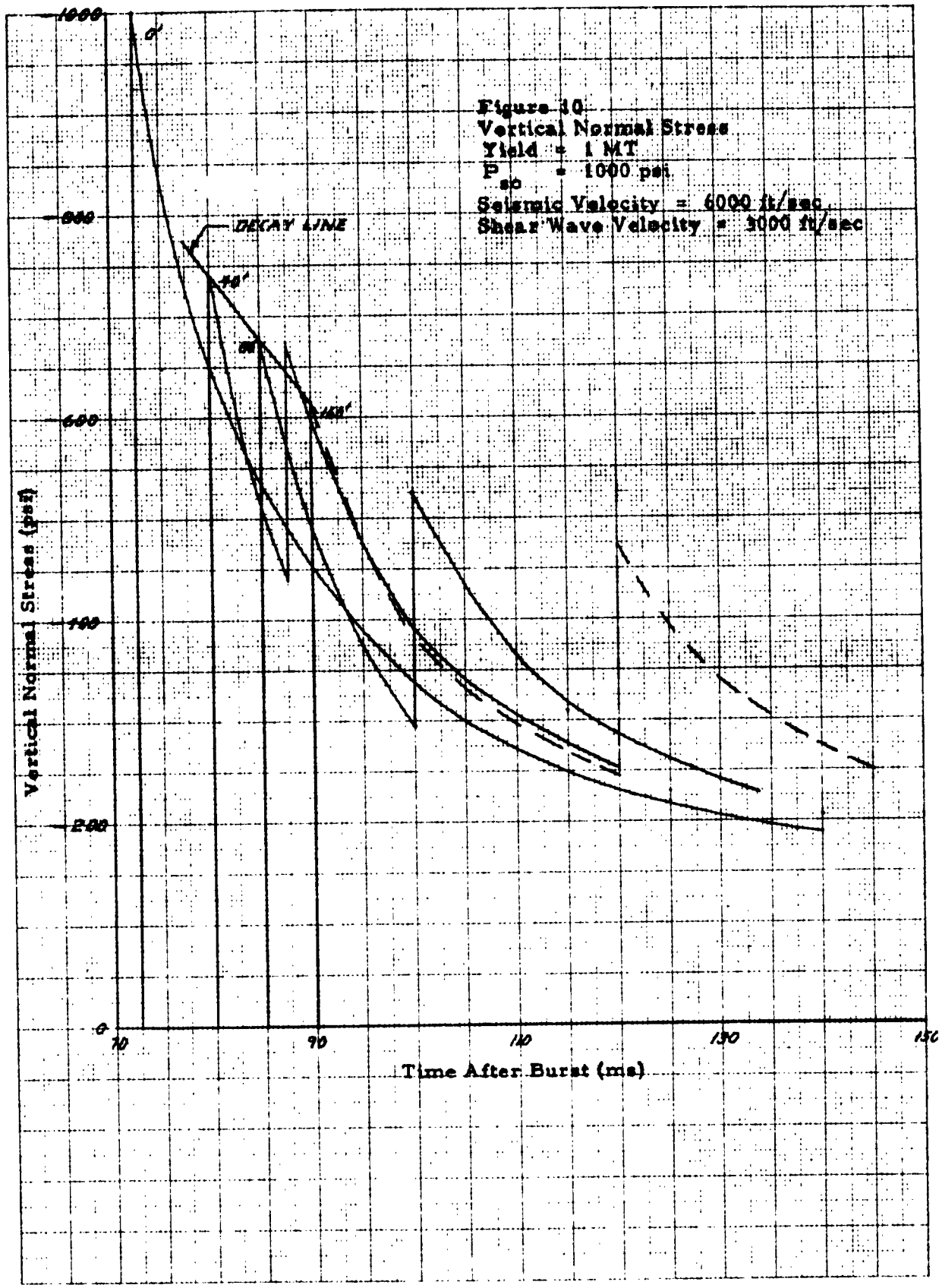
Figure 10
Vertical Normal Stress
Yield = 1 MT
P_{so} = 1000 psi
Seismic Velocity = 6000 ft/sec
Shear Wave Velocity = 3000 ft/sec
DECAY LINE
Vertical Normal Stress (psf)
Time After Burst (ms)
1000
800
600
400
200
0
70
90
110
130
150

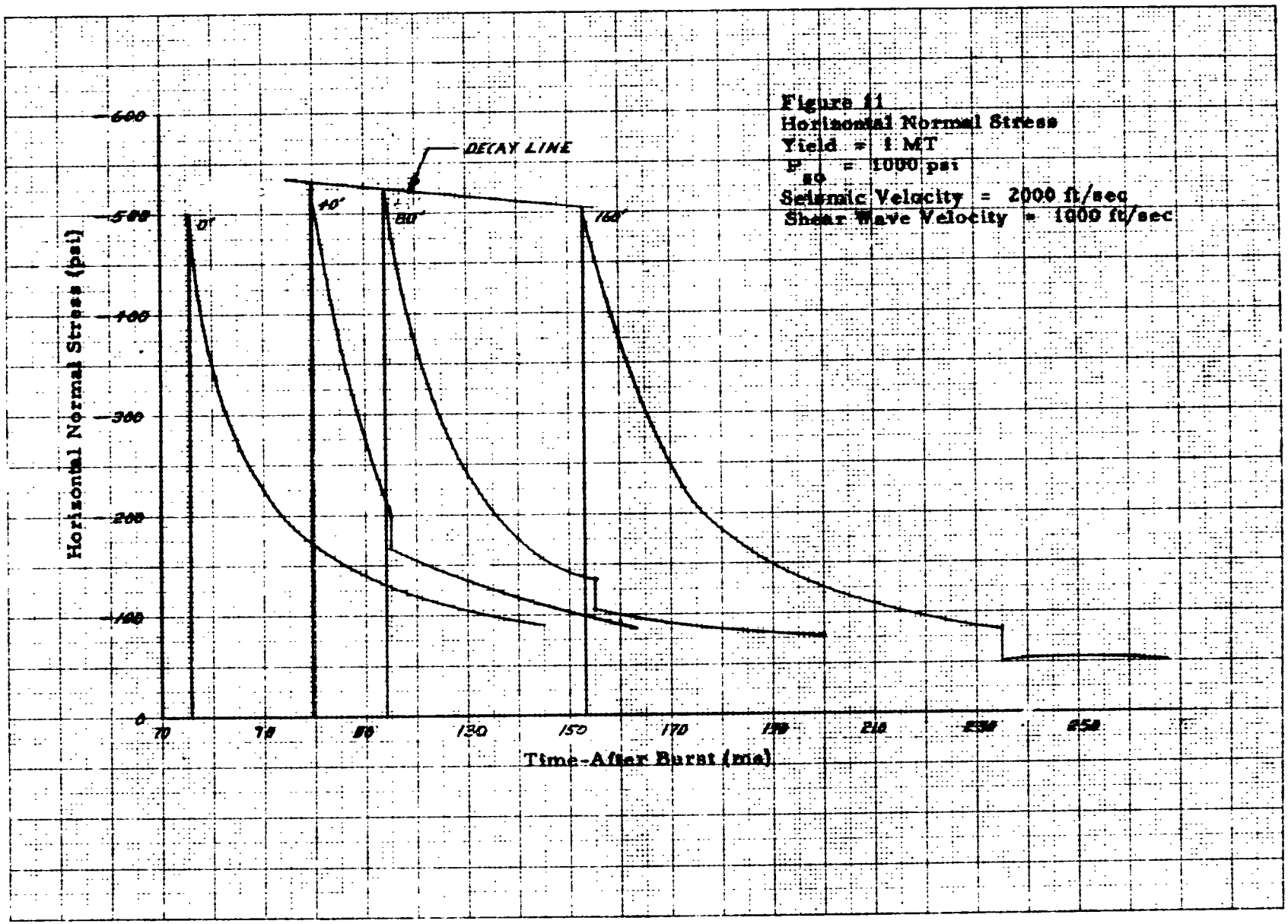

Figure 11
Horizontal Normal Stress
Yield = 1 MT
P_{so} = 1000 psi
Seismic Velocity = 2000 ft/sec
Shear Wave Velocity = 1000 ft/sec

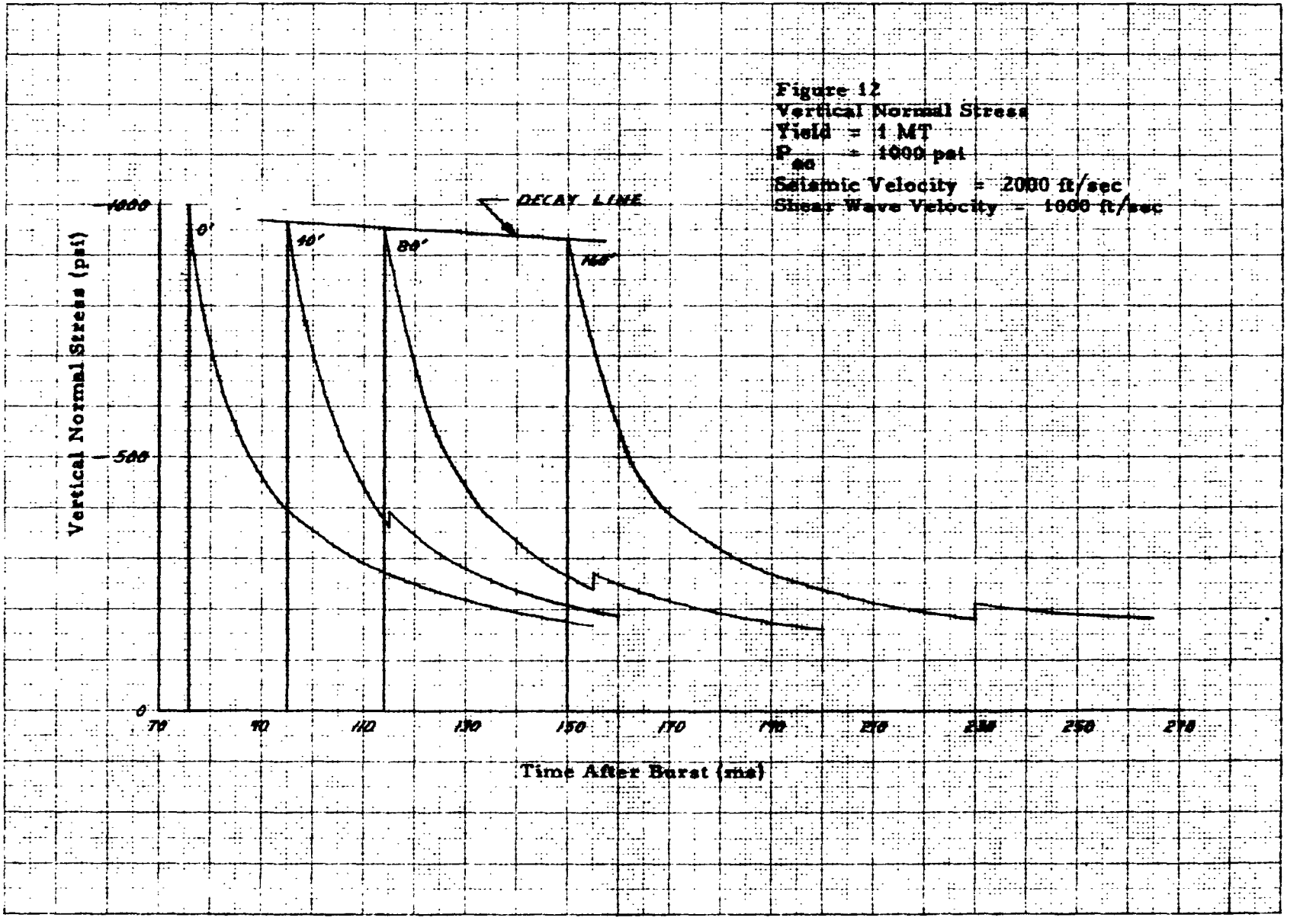

CHAPTER VIII

TYPICAL SOIL AND ROCK PROPERTIES

It is difficult to assign physical properties to earth materials by name since wide variations exist among different deposits of nominally the same material. In addition, considerable variations can be found in properties of samples from the same deposit. For this reason, data concerning such properties usually are given in extensive compilations which show the range of variation of these properties. Such presentations generally are limited to rock property data since presenting representative information for soils is far more difficult than for rocks. For this reason,only typical rock properties are tabulated here; soil properties are discussed only briefly and some basis is given for the choice of properties for analysis of ground stresses and motions.

A. ROCK PROPERTIES

Table 1 shows average properties of representative sound samples of typical rocks. These properties were obtained in various laboratory tests, primarily those of the U. S. Bureau of Mines, summarized in Appendix F of Volume IV. Average unit weight values show small variations; velocity, modulus, and compressive strength values are reliable within about ± 50 percent; Poisson's ratio values are questionable since some of the data showed negative values. Shear wave velocities were calculated from dilatational wave velocities and Poisson's ratio and tend to be less reliable than the other properties.

The indicated moduli and velocities tend to be too high for any near-surface deposit because of weathering and other surface effects. For moderately weathered or otherwise imperfect rock masses, a factor of about one-half should be applied to velocity and modulus of elasticity. This approach is somewhat crude, but the use to which the data are being put renders such an approach possible. For the 5,000 psi peak surface overpressure level, for example, both the AMF and SRI analytical results at all depths show small differences in response or stress for fairly large changes in seismic velocity above 6,000 ft/sec (if the situation remains superseismic). Because of the insensitivity of the analytical techniques

to variations in elastic properties in this range, as well as on the fairly small spread of properties among various types of rock, it is suggested that standard properties be assumed for any rock deposit. The choice largely depends on the condition of the rock. Reasonable values for these properties for sound hard rock would be: c_p = 15,000 ft/sec, c_s = 10,000 ft/sec, and ρ = 5.3 slugs/ft^3. For moderately weathered, or otherwise altered rock, these values would be: c_p = 8,000 ft/sec, c_s = 5,000 ft/sec, ρ = 5.3 slugs/ft^3. For soft or highly weathered materials, c_p = 6,000 ft/sec, c_s = 4,000 ft/sec, ρ = 5.0 slugs/ft^3. In general, dynamic and viscoelastic effects can be disregarded without serious error as can moisture content. Tectonic stresses probably are important for deep structures but are unknown and must be neglected. This introduces a large uncertainty in the knowledge of rock properties at deep locations.

B. SOIL PROPERTIES

Information regarding soil properties cannot be tabulated as simply as rock property data both because there is a great scarcity of published data and because measured soil properties depend more strongly on testing and sampling methods. Therefore, it is preferable to discuss the behavior of various soil types of interest and to attempt to conclude reasonable properties rather than to tabulate average values of measured properties. A thorough discussion of methods of arriving at suitable values of soil properties is given in "Nuclear Geoplosics , Vol. II, Mechanical Properties of Earth Materials", by R. V. Whitman.

The types of soils to be considered might be classified as saturated or partially saturated soils, and dry soils, either granular or cohesive. Saturated, or nearly saturated soils can be treated quite simply from the point of view of structure design. Air-induced stresses are transmitted almost entirely by water; therefore, stresses at shallow depths are the same as at the surface. Furthermore, horizontal stresses are equal to vertical stresses because the soil behaves essentially as a fluid. Seismic velocity is about 5,000 ft/sec (slightly above that for water); shear effects are small. The crater radius for a surface burst in wet soil is considerably larger than for the same material in a dry state; therefore, even disregarding increased construction costs, wet or saturated deposits appear to be undesirable as sites for shallow buried structures. Experience with saturated

deposits at the Pacific proving grounds (PPG) indicates that directly-transmitted stresses predominate below the water table (which is only a few feet below the ground surface at PPG) well beyond the close-in region. This tends to produce loads on the portions of structures located below the water table which are greater than the air-induced loads; reflections could cause further increases. Hence, saturated soils are not included in the following discussion.

Elastic properties of sand and other granular materials vary widely; however, normal density may be taken as 100 lb/ft^3 and Poisson's ratio may be taken as 1/3 for design purposes. Measured seismic velocities on the order of 500 ft/sec are mentioned by Whitman for near-surface sand deposits. He also reports elastic moduli (for zero lateral strain) which correspond to seismic velocities of about 2,000 ft/sec at high stress levels (about 2,000 psi). This appears to be a maximum value obtained in such tests since the modulus decreases slightly for higher stresses. Values for silt, such as that at the Nevada test site, are about 1,500 ft/sec, whereas clays show velocities of from 1,000 to 1,500 ft/sec. For materials which can be classified as low-grade rocks or highly-cemented soils, (e.g., shale, sandstone, and siltstone), Whitman reports values of dilatational velocity ranging from 2,500 ft/sec to 7,000 ft/sec.

It is suggested that the following values be used for estimating ground motions and stresses for dry or nearly-dry soils: for loose granular materials and clays, c_p = 1,000 ft/sec; for well-compacted granular materials and slightly-cemented materials, c_p = 2,000 ft/sec; for well-cemented materials, c_p = 4,000 ft/sec.

TABLE I

TYPICAL ROCK PROPERTIES

Rock	ρ (lb-sec^2/ft^4)	c_p (ft/ms)	c_s* (ft/ms)	E (lb/in^2)	ν	σ_c (lb/in^2)
Basalt	5.6	15	10	8×10^6	0.15	3.0×10^4
Dolomite	5.3	15	10	10×10^6	0.10	2.0×10^4
Gneiss	5.6	15	9	8×10^6	0.25	3.0×10^4
Granite	5.3	12	8	4×10^6	0.10	3.0×10^4
Limestone	5.3	15	10	8×10^6	0.20	2.0×10^4
Quartzite	6.4	17	12	12×10^6	0.15	5.0×10^4
Sandstone	4.8	8	8	2×10^6	0	1.5×10^4
Schist	5.6	15	10	8×10^6	0.10	2.5×10^4
Shale	5.5	10	7	5×10^6	0.10	1.5×10^4
Siltstone	5.5	14	9	7×10^6	0.10	2.0×10^4
Tuff (hard)	5.6	18	12	12×10^6	0.15	4.0×10^4
Tuff (soft)	4.8	8	4	2×10^6	0.10	1.5×10^4

ρ = density

c_p = dilatational wave velocity

c_s = shear wave velocity

E = Young's modulus

ν = Poisson's ratio

σ_c = compressive strength

*c_s values are calculated from measured values of E and ν

CHAPTER IX

SAMPLE DESIGN COMPUTATIONS

The purpose of this chapter is to show ways in which the data presented in earlier chapters of this report can be applied to the design of underground structures. For this reason, emphasis is placed on the discussion of the free field phenomena rather than on the proportioning of various types of structures. Furthermore, the discussion is limited to three types of structures: a deep tunnel in rock, either lined or unlined; a silo in well-compacted soil; a box-type structure at shallow depth (on the order of its span). These structures are discussed separately in the following sections; the discussions use as a starting point the comments of Chapter III concerning the application of analytical results to design.

A. SILO

The silo design consists of two parts: 1) the door (and closure) system design, and 2) the design of the silo itself. Although the door system design presents difficulties, it will not be considered here because the loads arise directly from air blast rather than from ground effects.

The stresses in the silo arise from the door loads, lateral earth loads, friction forces resulting from relative lateral displacements of the longitudinal axis of the silo. These stresses do not all occur simultaneously although there are combined effects; each of these effects is considered separately with only brief comments regarding possible combined effects.

The dimensions of the silo are taken to be as follows: length = 80 feet, inner radius = 6 feet. There is assumed to be no gallery at the surface and no superstructure protruding above the ground surface. The soil in which the silo is located is assumed to have the following properties: c_p = 2,000 ft/sec, c_s = 1,000 ft/sec ρ = 3.1 slugs/ft^3, zero cohesion, angle of internal friction = 30 degrees.

1. Design For Door Load

The door load is the best known of the loads for which the silo must be designed. This load, P, is the product of the peak surface overpressure, P_{so}, and the area of the top of the silo. It is assumed that the concrete used will be of high strength and will be reinforced; furthermore, there will be a steel inner liner to prevent spalling of concrete into the silo or other failures at the inner surface of the concrete. The allowable strength of reinforced concrete in the silo can be established as an average strength, σ_y, from the following expression:

$$\sigma_y = p\sigma_{st} + (1 - p)\,\sigma_c$$

where σ_{st} is the steel allowable stress, p is the steel percentage, and σ_c is the concrete allowable stress. Then equilibrium requires that:

$$P_{so}\,(\pi\, c^2) = \left[p\,\sigma_{st} + (1 - p)\sigma_c\right]\,\pi\,(c^2 - a^2) = \sigma_y\,\pi(c^2 - a^2). \tag{1}$$

Where a and c are the inner and outer radii of the silo, respectively, and P_{so} is the peak surface overpressure. Solving for the outer radius of the silo, c:

$$c = \sqrt{\frac{\left[p\,\sigma_{st} + (1 - p)\sigma_c\right]\,a^2}{\left[p\,\sigma_{st} + (1 - p)\sigma_c\right] - P_{so}}} = \sqrt{\frac{\sigma_y\,a^2}{\sigma_y - P_{so}}} \tag{2}$$

$$c = \frac{72 \text{ inches}}{\sqrt{1 - P_{so}/\sigma_y}} \tag{3}$$

Based on the results of analytical and experimental investigations of dynamic response of columns described in "The Dynamic Behavior of Reinforced Concrete Columns", Part III, by C. Y. Yang and K. F. Reinschmidt, Dept. of Civil Eng., MIT, October 1962, buckling is not a consideration for a silo of the dimensions used here, and the response of the silo to door loads will not differ greatly from the static case. Therefore, the above expressions, which are primarily for the static case, are applicable to the design of a silo for dynamic loads. The use of the surface peak overpressure as input to the silo without consideration of the door response is justified because the inertia of the door is negligible compared with the peak surface overpressure in the close-in region.

As an example of a design based on Equations (1) through (3), assume that the allowable concrete stress σ_c (using 0.85 f'_c to allow for creep and shrinkage) = 5,000 psi, allowable steel stress, σ_{st} = 50,000 psi, p = 0.05, a = 72 inches, P_{so} = 1,000 psi. Then, the allowable average stress σ_y is

$$\sigma_y = (0.05)\ (5,000) + (0.95)\ (50,000) = 7,250 \text{ psi}$$

and, from Equation (3)

$$c = \frac{72 \text{ inches}}{\sqrt{1 - 1,000/7,250}} = 78 \text{ inches}$$

or the required thickness of concrete is 6 inches. The location of the steel is not important for the door-load design, it can be distributed between reinforcing bars and inner liner in any proportion. Other factors will control this aspect. The allowable stresses used here are not recommendations but merely convenient values used to demonstrate the use of the data. The results, of course, are not to be considered as establishing the design of the silo.

2. Design For Lateral Loads

There are three aspects to the design of the silo to resist lateral loads. First there are the squeezing loads which give rise to uniform radial and tangential ring

stresses in the silo. Next, non-uniformity of the stress field at any given depth give rise to bending ring stresses. Finally, longitudinal bending stresses are induced because of the longitudinal non-uniformity of both applied loads and support conditions. The first two aspects of the design are considered here; longitudinal bending is treated in the following section.

A large amount of empirical evidence (from field tests of buried structures subjected to ground effects of nuclear weapons) indicates that the upper limit of the stress that can act on a buried structure is the free medium stress. The structure stresses only approach the medium stresses when the structure is more resistant to motion (or deformation) than the surrounding medium. There is also analytical evidence which supports this conclusion. On this basis, the problem of soil-structure interaction can be eliminated from consideration and the free medium stresses used as the loads on the silo.

Ring bending of the silo due to non-uniform radial stresses is considered next. Because no information regarding the distribution can be obtained from the AMF data (no tangential stresses), SRI results are used to demonstrate the variation of radial stresses on the silo at various depths at given times. Results of the SRI computations show that radial and tangential stresses are about equal at all depths and pressure levels for seismic velocities of 6,000 ft/sec or less. Thus the horizontal stress field is almost uniform, as is the distribution of normal stress on the silo. The small variation from uniformity of the distribution of normal stresses will not produce significant bending stresses.

The analysis of the silo as a ring reduces to considering only uniform normal stresses on the outer surface of the ring. Assuming elastic response, and that the configuration of the silo consists of a thick concrete ring with a thin steel liner, an expression for the required thicknesses of steel and concrete can be obtained by equating radial displacements of steel and concrete at the interface as follows:

$$U_r\Big|_{r=b}^{\text{conc.}} = U_r\Big|_{r=b}^{\text{steel}}$$

$$\frac{(1-\nu_c)b\,(b^2 p_b' - c^2 p_c) + (1+\nu_c)(b\,c^2)(p_b - p_c)}{E_c\,(c^2 - b^2)} = \frac{p_b(a+b)}{2E_s t} = \frac{f_s}{E_s} \qquad (4)$$

Where ν_c = Poisson's ratio for concrete = 0.15, E_c = Young's modulus for concrete = 3×10^6 psi, E_s = Young's modulus for steel = 30×10^6 psi, a is the inner radius, b is the interface radius, c is the outer radius, f_s is the allowable stress in the steel and t is the thickness of the steel liner. Equation (4) can be simplified with only small loss of accuracy by assuming $a = b$. Then solving for c gives

$$c = \sqrt{\frac{f_s a^2 (a + \nu nt - nt)}{f_s (a + \nu nt - nt) - 2 p_o na}} \qquad (5)$$

where $n = E_s/E_c = 10$.

As an example, take f_s = 50,000 psi, t = 0.2 inch, a = 72 inches, and P_{so} = 1,000 psi. From Figure 11 (page 19), the maximum horizontal stress is about 540 psi. Substituting these values in Equation (5) gives c = 79 inches or, in other words, the required concrete thickness is about 7 inches. In this case the steel stress governs the design. The concrete stress can be found from Equation (4) or by finding the interface stress, p_a and using this in the thick-walled cylinder equation as follows:

$$\sigma_\theta = \frac{p_a a^2 - p_c c^2 - (p_c - p_a)c^2}{(c^2 - a^2)} \qquad (6)$$

For this case, $p_a = f_s t/a = 139$ psi, $p_c = 540$ psi, $c = 79$ inches, $a = 72$ inches and σ_θ is found to be only 4820 psi. This is an inefficient use of concrete and better ratios of steel thickness to concrete thickness can be found. However, it is apparent from the above computations that the door-load stresses are more severe than ring stresses and, therefore, the ring stresses will not control the design.

3. Design For Friction Loads

Vertical friction loads on the structure come about because of the relative vertical motion of the silo and the surrounding medium. The amount of friction force depends on the relative vertical movement and also on the coefficient of friction between soil and concrete. This coefficient of friction is difficult to assess and, to avoid merely guessing at a suitable value, an alternate approach will be used which is based on the fact that the maximum vertical shear acting on the silo cannot exceed the shearing strength of the soil.

Soil shearing strength can be determined from the equation of the envelope of Morh's circles as follows:

$$s = c + p \tan \phi \qquad (7)$$

where s is the shearing stress at failure, c is the internal cohesion, p is the confining pressure, and ϕ is the angle of internal friction. For soils of interest here the cohesion, c, is only a few lb/in.^{2} and is negligible for high confining stresses. As previously stated, a good working value of about 0.6 (i.e., $\phi = 30$ degrees) appears to be reasonable. These values are for low stress levels, however, and are undoubtedly higher than values of tan ϕ for the same materials at higher stress levels. This is because the Mohr's circle is actually not a straight line but a concave-upward curve the slope of which (corresponding to tan ϕ) can become very small for large confining stresses. On this basis the value of tan ϕ will be reduced to 0.5 in this example.

The vertical stress in the silo is a function of the friction forces along the loaded length of the silo. It is apparent that the maximum vertical stress in the silo occurs at the lower end of the silo when the wave front has just arrived at this level. The upper limit of this stress is the sum of all the friction forces acting on the silo at the time of arrival of the air-induced stress at the bottom of the silo.

The total stress in the silo at the bottom is found by integrating the stresses over the surface and dividing by the cross-sectional area of the silo. The expression for the vertical stress, σ_z, at any depth, d, is as follows:

$$\sigma_z = \frac{(2\pi c \int_o^d \sigma_H \, d_z) \tan \phi}{\pi (c^2 - a^2)} = \frac{2c \tan \phi}{c^2 - a^2} \int_o^d \sigma_H \, d_z \qquad (8)$$

The variation of horizontal stress with depth required to evaluate $\int \sigma_H d_z$ is determined from interpolation of the curves of Figure 11* for 0, 40, and 80 feet. At the time the pulse arrives at 80 feet, the horizontal stress at the surface is 130 psi, the stress at 40 feet is 215 psi, and the stress at 80 feet is 520 psi. The simplest means of integrating ($\sigma_H d_z$) is by sketching the horizontal-stress versus depth curve on graph paper and counting unit areas. This has been done for the case under consideration as shown in Figure 13; the total horizontal force determined from this figure is about 240,000 lbs.

Equation (8) can be put into a form more useful by solving of the required outer radius, c. This gives

$$c = \sqrt{a^2 + \left(\frac{F \tan \phi}{\sigma_y}\right)^2} + \frac{F \tan \phi}{\sigma_y} \qquad (9)$$

where $F = \int \sigma_H d_z$ = the total horizontal force on the silo.

* Page 19

Computation of σ_y in this case differs from that for door loads in that an increase in allowable concrete stress should be included here because of confinement effects. On the basis of experimental evidence the cylinder strength, f'_c, can be increased by an amount equal to four times the minimum principal stress* or three-fourths of the intermediate principal stress.** No discussion is given here of the data on which these increases are based; the results are used merely for illustration.

To find the required outer radius,c, from Equation (9), the known (or assumed) values of a = 72 inches, tan ϕ = 0.5, F = 240,000 lbs are substituted together with the value of σ_y determined from allowable steel and concrete stresses and percent steel. Allowable concrete stress is a function of the thicknesses of concrete and steel, which makes use of Equation (9) in design rather difficult. It is perhaps preferable to assign values to σ_y and calculate c than to adjust the required steel percentage on the basis of the allowable concrete stress. Based on the value of σ_y determined for the door load, σ_y = 8,000 psi appears to be a reasonable value for friction loads. Substituting this in Equation (9) gives c = 87 inches, or required thickness = 15 inches.

In this case the friction stresses apparently are more severe than the door load stresses and control the design for axial loads. For higher overpressure levels this probably would not be the case, furthermore, an extremely conservative approach has been made to friction loads. It is suggested that the shear strength of the backfill material be checked carefully and altered, if necessary, to reduce friction-induced stresses in cases in which these stresses control the design. It might be possible, as an alternative, to lubricate the silo to reduce these stresses. Such techniques are in the designers realm and are not germane to the discussion of free field effects.

* "A Study of the Failure of Concrete Under Combined Compressive Stresses", F. Richart, A. Brandtsaeg, and R. L. Brown, Bull. No. 185, Univ. of Ill. Eng. Exp. Sta., 1928.

** "Strength of Concrete Under Combined Stress", C. J. Bellamy, Journal, Amer. Conc. Institute, October 1961, pp. 367-381.

4. Design for Bending Loads

Two extreme models are considered in examining bending effects: 1) a compliant structure, the curvatures of which match the curvatures of a vertical line in the soil, and 2) a stiff structure loaded by the free-field horizontal stresses.

If the silo is assumed to be perfectly compliant, bending moments in the silo are obtained directly from the soil vertical-line curvature from the strength of materials relationship,

$$M = EI \left(\frac{\partial^2 u_r}{\partial z^2} \right) \tag{10}$$

in which EI represents the bending stiffness of the silo structure and $\frac{\partial^2 u_r}{\partial z^2}$ is an approximation to the free-field curvature of a vertical line in the soil. For a constant-section silo, therefore, the distribution of bending moments along the length of the silo is directly proportional to the curvature of a vertical line in the soil. The variation of shear, V, and lateral load, q, along the length of silo are obtained from the differential equilibrium relationships.

$$V = \frac{dM}{dz} \tag{11}$$

$$q = \frac{dV}{dz} = \frac{d^2M}{dz^2} \tag{12}$$

To examine the consequences of the assumption of compliance, take the case of P_{so} = 5,000 psi, c_p = 12,000 ft/sec, silo length = 80 feet; then 6.67 ms are required for the pulse to travel the length of the silo. The curvatures (obtained from Figure 5.8 of Appendix C) and the resulting bending moments, shears, and loads (obtained from Equations 10, 11, and 12, respectively) are shown in Figure 14. Although it is possible to design the silo for these stresses, it should be noted that the assumption of a compliant silo leads to large concentrated moments and forces which are difficult to justify, particularly if the structure has any appreciable longitudinal stiffness.

To design for free field horizontal stresses, the silo is treated as a rigid beam supported by an elastic foundation. This assumption permits computation of reactive soil pressures directly from equilibrium considerations. As the pressure pulse moves down through the soil, the silo is loaded by unbalanced horizontal stresses which arise due to the phase lag between the upstream and downstream sides of the silo. To simplify the loading on the silo, an equivalent square silo can be used. The horizontal stress curves of Chapter VII can be used to determine the loads.

If the base of the silo is firmly imbedded in a very hard material (i.e., it can be assumed that relative translation is prevented and that the soil provides essentially a hinge support to the silo at its base), than the support conditions consist of an elastic foundation and a hinged base. If the soil is assumed to be incapable of providing a concentrated reaction the support conditions will be simply that of an elastic foundation the reaction of which is proportional to the displacement. In either case, equilibrium equations for moments and forces lead to the determination of the reactions at any time. Then shear and bending moment can be calculated for each of several positions of the wave front and the maximum values of shear and moment chosen for design.

For an example, take P_{so} = 5,000 psi and c_p = 2,000 ft/sec and assume that the silo is hinged at the bottom. Then the variation of the maximum soil reaction at the top of the silo is as shown in Figure 15 as are the shear and bending moment diagrams for various wave-front locations (only a few locations are shown for illustration) in Figure 15; more were used to actually find the maximum moment and shear). The maximum bending moment is 32,800 inch-kips per inch of diameter. Both occur when the wave front is 48 feet from the top of the (80-foot) silo. Maximum soil pressure is 662 psi and occurs at the top of the silo (based on the assumption of linear displacement). For a silo with a = 72 inches and c = 108 inches, the average shear stress is

$$\tau = \frac{V}{\text{area}} = \frac{86{,}700 \text{ lb/in.} \times 216 \text{ in.}}{\pi (108^2 - 72^2)} = 920 \text{ psi}$$

and the maximum bending stress is

$$\sigma_{max} = \frac{Mc}{I} = \frac{(32.8 \times 10^6 \times 216)(108)}{8.57 \times 10^7} = 8{,}940 \text{ psi.}$$

For no concentrated reaction at the bottom, the corresponding values are τ = 1,510 psi and σ_{max} = 7,950 psi. The actual design of the silo can proceed from these values on the basis of usual straight time reinforced concrete theory.

B. DESIGN OF DEEP TUNNELS IN ROCK

In the case of deep tunnels, the necessary information for rational design is lacking; therefore, this section will consist primarily of comments regarding the possible approaches to the problem. Two modes of failure are discussed: spalling and crushing. The former is primarily a function of geometry of both wave and tunnel and the latter is mostly dependent on stress level. In discussing these modes of failure residual or tectonic stresses are disregarded mostly because there is so little available information on these potentially important stresses.

The first mode of failure to be discussed is spalling. Based on the study of Logcher, as discussed in Chapter III, it is difficult for spalling to occur in a circular opening for any pulse except one with a very short rise time and a duration not more than about the time of transit of the pulse across the opening. On the other hand, the pulses obtained from the analyses of Brooks and Newmark are rather rounded and of fairly long duration (i.e., 50 ms or more for moderate depths). For 6,000 ft/sec material, as used by Newmark in his analysis, a 50 ms transit time corresponds to a 300 ft diameter tunnel. By neglecting geometry of the opening and considering a rod model, the effect of pulse shape on spall length can be studied. The relationship of spall thickness to spall length for various ratios of ultimate tensile strength to peak stress is shown in Figure 16. For example, if the ultimate tensile stress is taken as 0.4 times the peak pressure, the length of a spall for a zero rise time is 0.2 times the length of the pulse. If a rise time equal to 0.3 times the duration of the pulse (i.e., A/L = 0.3) is used, the length of the spall is 0.44 times the length of the pulse.

To illustrate the use of this figure with data from the Newmark analysis, consider the time history of radial stress at 1,000 ft below a 2 MT burst. (Figure 49, Chapter IV). The peak stress is about 40 ksi and the rise time is about 30 ms, whereas the

duration is about 60 ms. Assuming that the tensile strength of the rock is small ($k = 0$), the length of spall would be half the pulse length. For $c_p = 6{,}000$ ft/sec (the material used by Newmark) the spall length is one-half of 360 feet or 180 feet. Therefore, spalling could only occur for large diameter tunnels, even if tunnel geometry were neglected. The above comments do not consider spalling which occurs as a result of existing faults being mobilized. No means of treating such phenomena is now available.

The simplest criterion of failure by crushing is that the maximum tangential (compressive) stress at the tunnel surface equals the unconfined compressive strength of the rock (as discussed by Clark and Candle in Appendix G, a quasi-static approach to stresses at fairly large depths below megaton surface detonations is satisfactory). This criterion is based on the maximum stress theory or, in the case where the minimum lateral confining stress is zero, the Mohr failure theory. Thus if the free field compressive stress is σ_{ff}, the stress concentration factor is taken as 3.0, (which is the maximum value both static and dynamic for $\nu = 0.25$) and the ultimate compressive strength of the rock is σ_c, crushing failure takes place when

$$\sigma_{ff} = \frac{\sigma_c}{3} \quad .$$

If, in the above expression, the free field stress is only slightly in excess of the compressive strength of the rock divided by the stress concentration factor, little fragmentation would normally be expected. However, as the free field stress increases, the likelihood of fracture and fragmentation increases. As failure proceeds outward from the center of the tunnel, the shape of the tunnel changes and may result in a change of the stress concentration factor at the root of the failure, as discussed in Appendix G. The speed at which failure propagates into the rock can be assumed to be equal to the seismic velocity of the rock material.

Figure 17 is a schematic of fracture history in a long-period stress field superimposed on a static stress field. The duration of the super-critical stress field is represented by t_c. This duration multiplied by the shear velocity of the rock material is an index to the extent of crack propogation since failure is primarily a shear phenomena. However, collapse of the cavity may not be as extensive as crack

propogation because "keying in" of fragments and blocks may give sufficient support to reduce stress concentration until the free field stress is reduced.

The unconfined compressive strength and seismic velocity can be obtained from Table I or from the more extensive tabulation of Appendix F or Appendix G. As an example, take a soft tuff for which c_p = 8,000 ft/sec, c_s = 4,000 ft/sec and unconfined compressive strength σ_c is 15 ksi. The stress concentration factor is 3; assume that the time of overstress is 6 ms and the free field stress (i.e., static + dynamic) is 6,000 psi. The strength of the granite is exceeded by 3 x 6,000 - 15,000 = 3,000 psi for 8 ms. For unlined tunnels the amount of overstress is less important than the time during which overstressing occurs. In this example, therefore, cracks can propagate into the rock a distance of 24 feet.

The uses to which this result can be include determining length of required rock bolts to insure that no rock falls into the cavity either during loading or there after. Alternatively, a criterion for closure of the opening might be based on whether the crack propagates a distance equal to the radius of the tunnel. Empirical support for such a criterion is required.

A means of preventing even incipient failure for the overstressed condition lies in lining the tunnel, preferably with a steel liner, to reduce the tangential stress in the rock at the tunnel face. As was mentioned earlier for concrete, rock displays increased strength with increased lateral confinement. Thus the liner doubly improves the situation. The amount of increase of rock strength can be taken as three-fourths of the interface stress between steel and rock; therefore, a liner giving 1,000 psi interface stress (about 4 inches for a 35-ft diameter tunnel) would decrease the overstress by 750 psi. Theoretical results by Baron and Paines ("Further Studies on the Diffraction of a Pressure Wave by an Elastically Lined Cylindrical Cavity in an Elastic Medium", the MITRE Corporation, SR-72 Sept. 1962) indicate that a 4-inch steel liner in a 35-ft diameter tunnel would reduce the stress concentration factor by one-fourth. This alone would reduce the rock stress below the unconfined compressive stress; therefore,

a thinner liner would suffice. A cut and try approach to this problem seems adequate.

C. SHALLOW BOX-TYPE STRUCTURE

No reliable method of predicting loads on buried structures in soil has been developed, however, some means of estimating these loads are available. One of these considers the surfaces on which shear forces are mobilized because of deformation or displacements of the structure; the other considers the relative compressibility of the structure and the soil replaced by it. The latter approach is discussed briefly here; fairly extensive discussion of both methods is given in "Nuclear Geoplosics", Vol. V.

The relative-compressibility concept is based on the reduction of stress on a soil-structure interface if the interface can move away from the soil and thus mobilize the shear strength of the soil. Structures stiffer than the soil, on the other hand, experience loads greater than the free medium stresses. In practice, however, stresses larger than the free medium stresses have not been observed, and stresses much lower have been measured. Therefore, free medium stresses are a conservative estimate of the loads on buried structures.

The surrounding soil provides both damping and virtual mass to the responding elements of the box structure. The net result is reduction of dynamic effects. Furthermore, structural materials exhibit increased yield or ultimate strengths when subjected to rapid loading, which balances any increased dynamic response. Also any increased response increases the effective compressibility of the structure, thus decreasing the applied load. On this basis it appears that ignoring dynamic response does not render the approach unconservative. The free medium stresses can be applied as static loads for purposes of analysis and the resulting design will always be conservative if possibly wasteful of materials.

As an example, to design a structure 20 feet by 20 feet deep with the top surface at a depth of 40 feet for P_{so} = 1,000 psi and c_p = 2,000 ft/sec. From Figure 12,*

* See Page 20

the peak stress on the top face (i.e., the vertical normal stress at a depth of 40 feet) is 970 psi, and on the bottom is 960 psi. From Figure 11*, the average peak (horizontal) stress on the sides is 520 psi. Each of the faces can be designed for bending alone; a check of axial stresses, after design has been made for bending, will show rather small axial stresses. Each of the sides can be treated as a square clamped plate for which the maximum bending moment (which occurs at the edge of the plate), $M_{max} = 0.0513 \, p \, a^2$, where p is the average pressure against the side and a is the length of a side (= 20 feet in this case). The moment at the center of the side is 45 percent of the maximum moment. For the top side the two design moments are 2,870 in.-kips/in. and 1,290 in.-kips.inch. Design for these moments can be carried out using suitable material properties and thicknesses of materials.

* See Page 19

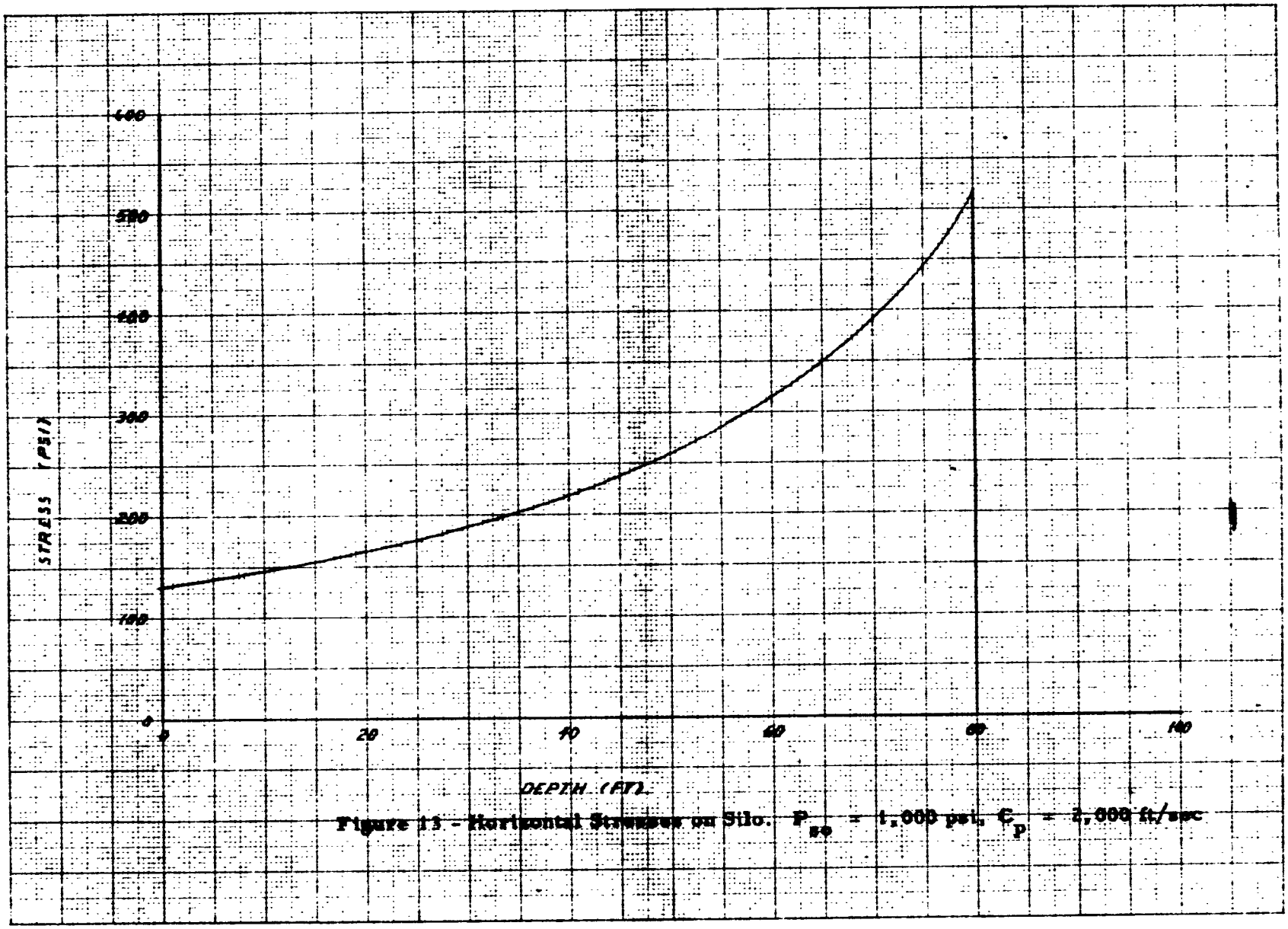

Figure 13 - Horizontal Stresses on Silo. P_{so} = 1,000 psi, C_p = 2,000 ft/sec

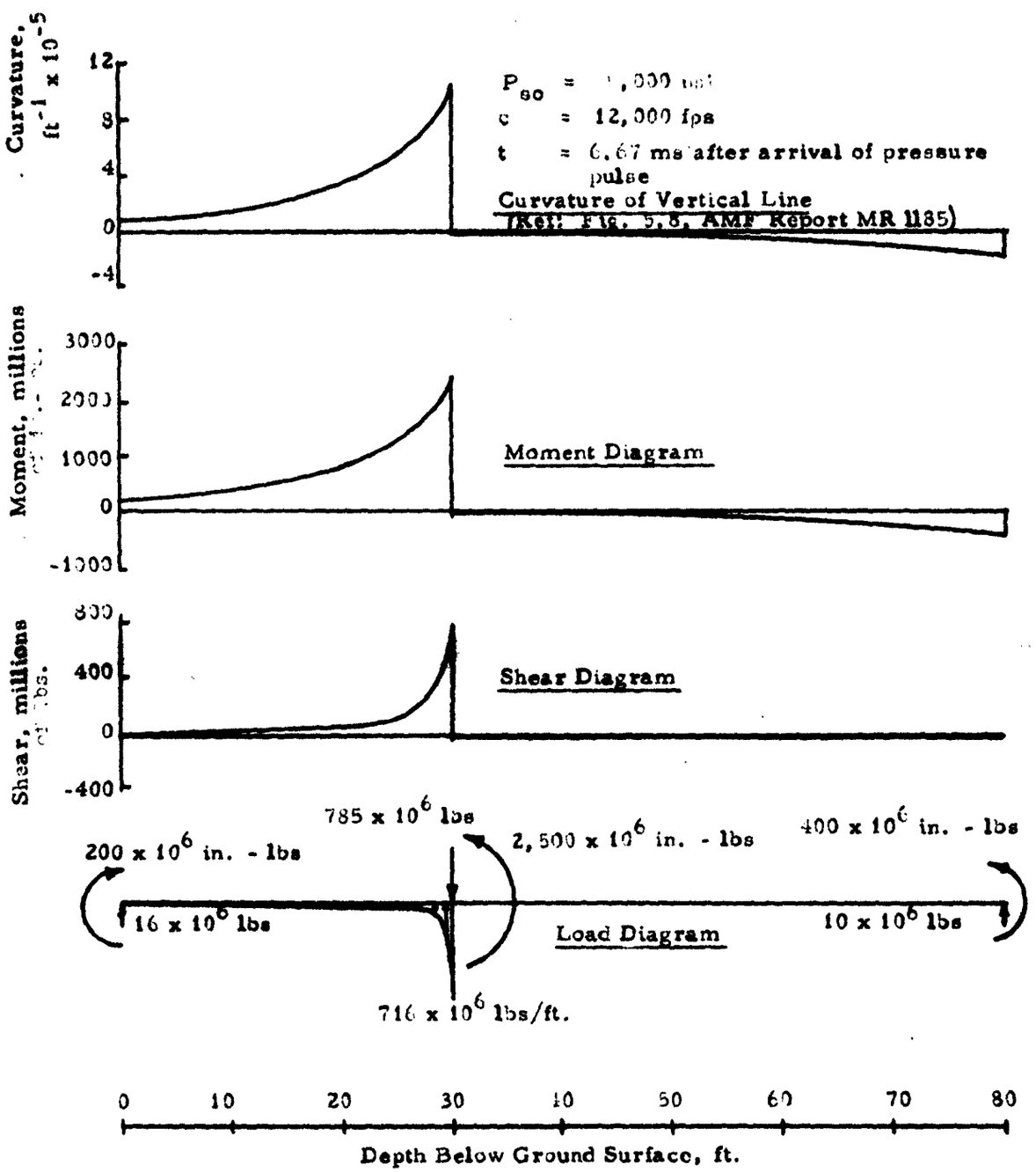

FIGURE 14 - Curvature, Moment, Shear, and Loading Diagrams for Compliant Silo Structure

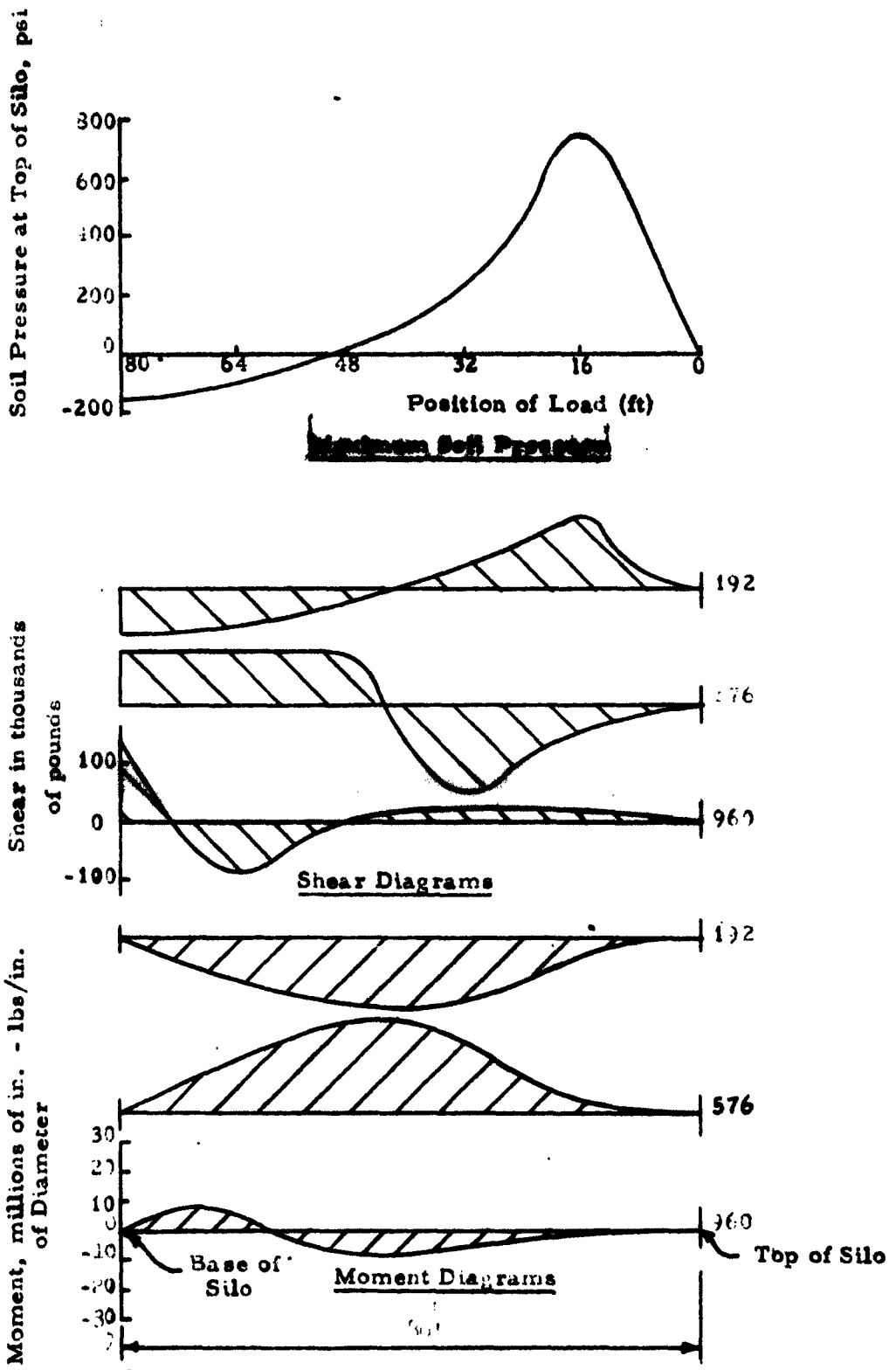

FIGURE 15 - Maximum Soil Pressure, Shear Diagrams, and Moment Diagrams for Silo on Elastic Foundation with a Hinged Base.

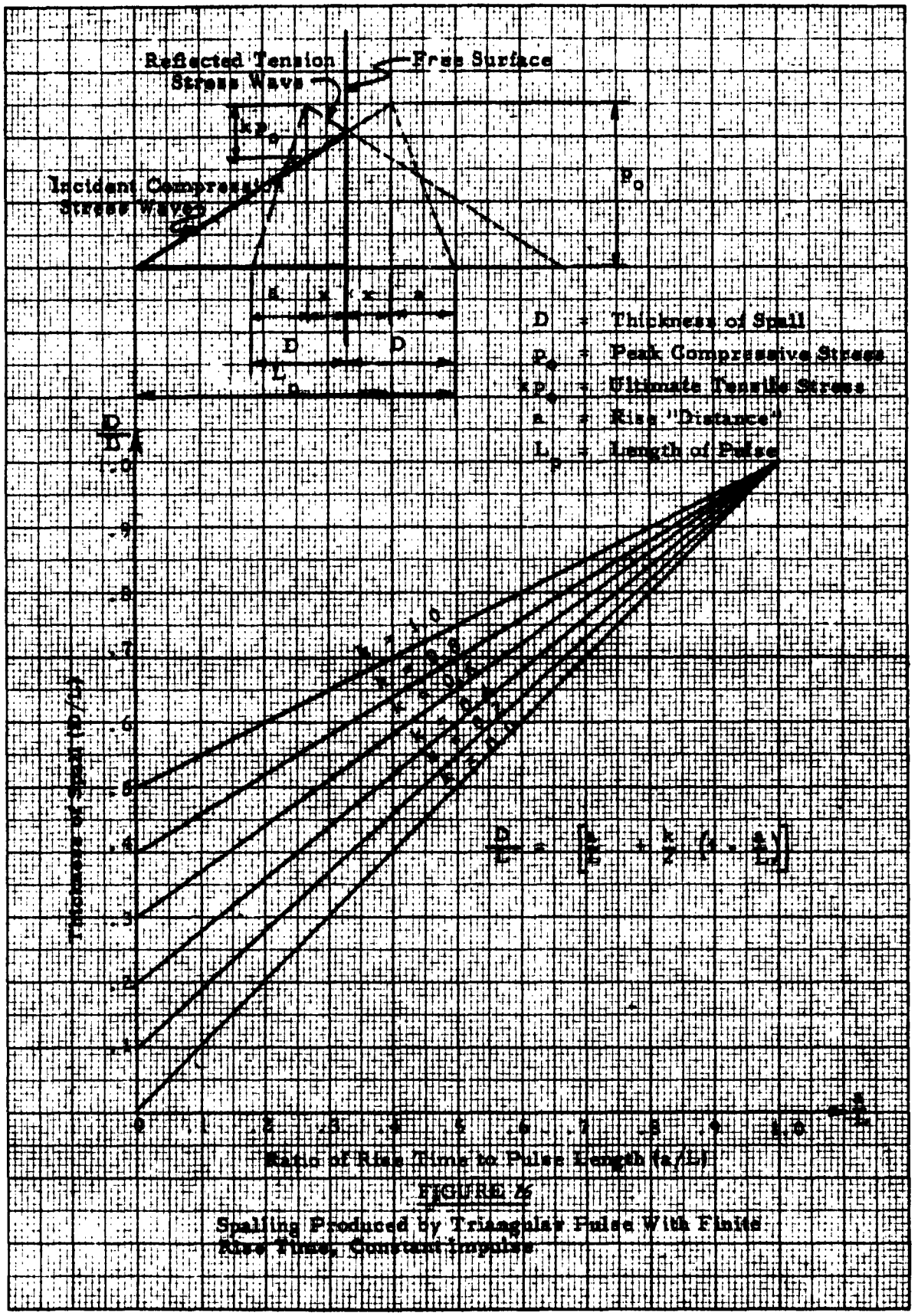

FIGURE 16

Spalling Produced by Triangular Pulses With Finite Rise Times, Constant Impulse

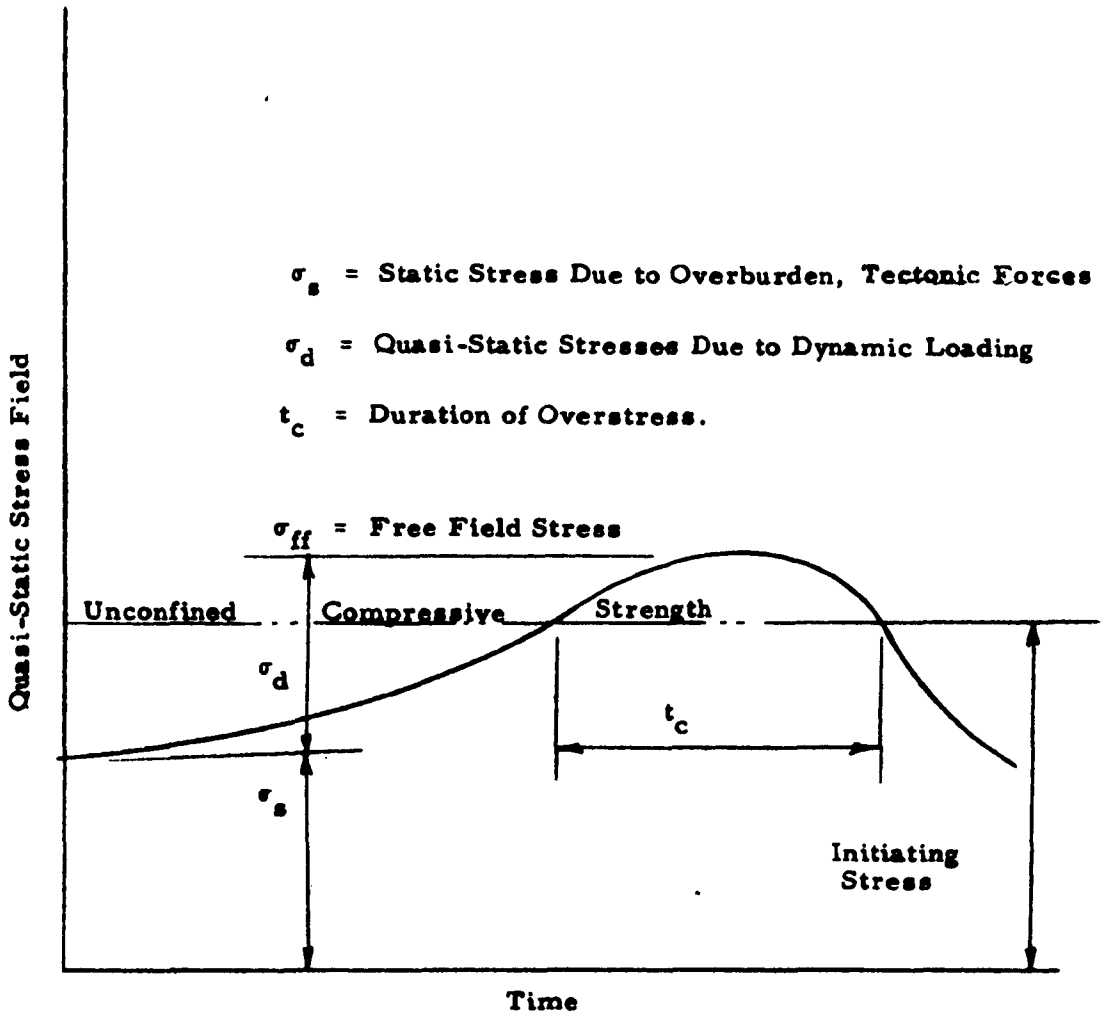

FIGURE 17

Schematic of Fracture History in a Long Period Stress Field Superimposed on A Static Stress Field

DISTRIBUTION LIST FOR

BLAST & SHOCK

R & D REPORTS

Revised 9 Nov. 1962

ADDRESSEE	ARMY	No. of Cys.
Chief of Research and Development, D/A, Washington 25, D. C. Attn: Atomic Division		1
Chief of Engineers, D/A, Washington 25, D. C.		
Attn:	ENGCW-NE	1
	ENGTE-E	1
	ENGMC-E	1
Commanding General, U. S. Army Materiel Command, Washington, D. C. Attn: AMCRD-DE-N		2
Commanding General, U. S. Continental Army Command, Ft. Monroe, Virginia		1
President, U. S. Army Air Defense Board, Ft. Bliss, Texas		1
Commandant, Command & General Staff College, Ft. Leavenworth, Kansas, Attn: Archieves		1
Commandant, U. S. Army Air Defense School, Ft. Bliss, Texas Attn: Command & Staff Dept.		1
Director, Special Weapons Development, Hq, CDC, Ft. Bliss, Texas, Attn: Chester I. Peterson		1
Commanding General, Aberdeen Proving Ground, Aberdeen, Md. Attn: Director, BRL		1
Commanding General, The Engineer Center, Ft. Belvoir, Va. Attn: Asst. Commandant, Engineer School		1
Director, U. S. Army Research and Development Laboratory Ft. Belvoir, Va. Attn: Chief, Tech. Support Branch		1
Commanding Officer, U. S. Army Mobility Command, Center Line, Michigan		1
Commanding Officer, Picatinny Arsenal, Dover, N. J. Attn: ORDBB-TK		1
Commanding Officer, Transportation Research Command, Ft. Eustis, Va., Attn: Chief, Tech. Info. Div.		1

ARMY CONT'D	No. of Cys.
Commanding General, USA Electronic R&D Lab., Ft. Monmouth N. J., Attn: Technical Documents Center, Evans Area	1
Commanding General USA Missile Command, Huntsville, Alabama	1
Commanding General, USA Munitions Command, Dover, New Jersey	1
Commanding Officer, U. S. Army Corps of Engineers, Beach Erosion Board, Washington, D. C.	1
Commanding Officer, U. S. Army Nuclear Defense Laboratory, Edgewood Arsenal, Edgewood, Md., Attn: Tech. Library	1
Director, Waterways Experiment Station, U. S. Army Corps of Engineers, Vicksburg, Mississippi, Attn: Library	1
Director, U. S. Army Corps of Engineers, Nuclear Cratering Group, Livermore, California	1
NAVY	
Chief of Naval Operations, ND, Washington 25, D. C.	
Attn: OP-75	2
Attn: OP-03EG	1
Director of Naval Intelligence, ND, Washington 25, D. C.	
Attn: OP-922V	1
Chief, Bureau of Naval Weapons, ND, Washington 25, D. C.	2
Chief, Bureau of Ships, ND, Washington 25, D. C.	
Attn: Code 372	1
Attn: Code 423	1
Chief, Bureau of Yards and Docks, ND, Washington 25, D. C.	
Attn: Code D-400	1
Attn: Code D-440	1
Chief of Naval Research, ND, Washington 25, D. C.	
Attn: Code 811	1
Commander-in-Chief, U. S. Pacific Fleet, FPO, San Francisco, California	1
Commander-in-Chief, U. S. Atlantic Fleet, U. S. Naval Base, Norfolk 11, Va.	1

NAVY CONT'D	No. of Cys.
Commandant of the Marine Corps, ND, Washington 25, D. C. Attn: Code A03H	4
President, U. S. Naval War College, Newport, R. I.	1
Superintendent, U. S. Naval Postgraduate School, Monterey, California	1
Commanding Officer, Nuclear Weapons Training Center, Atlantic, Naval Base, Norfolk 11, Va., Attn: Nuclear Warfare Dept.	1
Commanding Officer, U. S. Naval Schools Command, U. S. Naval Station Treasure Island, San Francisco, California	1
Commanding Officer, Nuclear Weapons Training Center, Pacific, Naval Station, North Island, San Diego 35, California	2
Commanding Officer, U. S. Naval Damage Control Training Center, Naval Base, Philadelphia 12, Pa., Attn: ABC Defense Course	1
Commander, U. S. Naval Ordnance Laboratory, Silver Spring 19, Md. Attn: EA Attn: EU Attn: E	 1 1 1
Commander, U. S. Naval Ordnance Test Station, China Lake, Calif.	1
Commanding Officer & Director, U. S. Naval Civil Engineering Laaoratory, Port Hueneme, Calif., Attn: Code L31	1
Director, U. S. Naval Research Laboratory, Washington 25, D. C.	1
Commanding Officer & Director, Naval Electronics Laboratory, San Diego 52, California	1
Commanding Officer, U. S. Naval Radiological Defense Laboratory, San Francisco, Calif., Attn: Tech. Info. Division	1
Commanding Officer & Director, David W. Taylor Model Basin, Washington 7, D. C., Attn: Library	1
Underwater Explosions Research Division, DTMB, Norfolk Naval Shipyard, Portsmouth, Virginia	1

AIR FORCE	No. of Cys.
Hq, USAF (AFDRC/NE - Maj. Lowry) Washington 25, D. C.	1
Deputy Chief of Staff, Plans and Programs, HQ USAF Washington 25, D. C., Attn: War Plans Division	1
Director of Research and Development DCS/D, Hq USAF, Washington 25, D. C., Attn: Guidance & Weapons Division	1
Air Force Intelligence Center, Hq USAF, ACS/I (AFCIN-3K2) Washington 25, D. C.	1
Commander-in-Chief, Strategic Air Command, Offutt AFB, Nebraska, Attn: OAWS	1
Commander, Tactical Air Command, Langley AFB, Virginia, Attn: Document Security Branch	1
ASD, Wright Patterson AFB, Ohio	1
Commander, Air Force Logistics Command, Wright-Patterson AFB, Ohio	2
AFSC, Andrews Air Force Base, Washington 25, D. C., Attn: RDRWA	1
Director, Air University Library, Maxwell AFB, Alabama	2
AFCRL, L. G. Hanscom Field, Bedford, Massachusetts Attn: CRQST-2	1
AFSWC (SWRS) Kirtland AFB, New Mexico	3
Commandant, Institute of Technology, Wright-Patterson AFB, Ohio, Attn: MCLI-ITRIDL	1
BSD, Norton AFB, California	1
Director, USAF Project RAND, Via: U. S. Air Force Liaison Office, The RAND Corporation, 1700 Main Street, Santa Monica, California	1
Director of Civil Engineering, Hq USAF, Washington 25, D. C. Attn: AFOCE	1

OTHERS	No. of Cys.
Director of Defense Research & Engineering, Washington 25, D. C. Attn: Tech. Library	1
U. S. Documents Officer, Office of the United States National Military Representative-SHAPE, APO-55, New York, N. Y.	1
Commander-in-Chief, Pacific, Fleet Post Office, San Francisco, California	1
Director, Weapons Systems Evaluation Group, OSD, Room 1E880, The Pentagon, Washington 25, D. C.	1
Commandant, Armed Forces Staff College, Norfolk 11, Virginia Attn: Library	1
Commander, Field Command, DASA, Sandia Base, Albuquerque, New Mexico	1
Commander, Field Command, DASA, Sandia Base, Albuquerque, New Mexico, Attn: FCWT	1
Attn: FCTG	1
Chief, Defense Atomic Support Agency, Washington 25, D. C.	5
Commandant, Army War College, Carlisle Barracks, Pensylvania Attn: Library	1
Commandant, National War College, Washington 25, D. C. Attn: Class Rec. Library	1
Commandant, The Industrial College of the Armed Forces, Ft. McNair, Washington 25, D. C.	1
Officer-in-Charge, U. S. Naval School, Civil Engineering Corps Officers, U. S. Naval Construction Battalion, Port Hueneme, California	1
Los Alamos Scientific Laboratory, P. O. Box 1663, Los Alamos, New Mexico, Attn: Report Librarian (for Dr. A. C. Graves)	1
Administrator, National Aeronautics & Space Administration 1512 H Street, N. W. Washington 25, D. C.	1
Langley Research Center, NASA, Langley Field, Hampton, Va. Attn: Mr. Philip Donely	1
Chief, Classified Technical Library, Technical Information Service, U. S. Atomic Energy Commission, Washington 25, D. C., Attn: Mrs. Jean O'Leary (for Dr. Paul C. Fine)	1

OTHERS CONT'D	No. of Cys.
Chief, Classified Technical Library, Technical Information Service U. S. Atomic Energy Commission, Washington 25, D. C., Attn: Mrs. Jean O'Leary	1
Dr. Walker Bleakney, Forestal Research Center Library, Aeronautical Sciences Bldg., Princeton University, Princeton, N. J., Attn: Librarian	1
Manager, Albuquerque Operations Office, U. S. Atomic Energy Commission, P. O. Box 5400, Albuquerque, New Mexico	1
Dr. Robert J. Hansen, Division of Industrial Cooperation, Massachusetts Institute of Technology, 77 Massachusetts Avenue, Cambridge, Massachusetts (Send TS to 244 Wood St. Lexington, Mass.)	1
Dr. Bruce G. Johnston, The University of Michigan, University Research Security Office, Lobby 1, East Engineering Bldg., Ann Arbor, Michigan (Do not send Top Secret to this addressee)	1
Sandia Corporation, Sandia Base, Albuquerque, New Mexico Attn: Classified Document Division (for Dr. M. L. Merritt)	1
Superintendent, Eastern Experiment Station, U. S. Bureau of Mines, College Park, Md., Attn: Dr. Leonard Obert (Underground Effects Only)	1
Dr. Nathan M. Newmark, University of Illinois, Room 207, Talbot Laboratory, Urbana, Illinois (No Top Secret to this addressee)	1
Commander, ASTIA, Arlington Hall Station, Arlington 12, Virginia, Attn: TIPDR (No Top Secret or Restricted Data to this addressee)	15
Holmes & Narver, Inc., AEC Facilities Division, 849 S. Broadway Los Angeles 14, California, Attn: Mr. Frank Galbreth	1
Professor Robert V. Whitman, Massachusetts Institute of Technology, Room 1-343, Cambridge 39, Massachusetts	1
Professor J. Neils Thompson, University of Texas, Structural Mechanics Research Laboratory, Austin, Texas	1
Mr. Kenneth Kaplan, United Research Services, 1811 Trousdale Drive, Burlingame, California	1
Mr. Fred M. Sauer, Department of Physics, Stanford Research Institute, Menlo Park, California	1

OTHERS CONT'D	No. of Cys.
Dr. Robert C. DeHart, Southwest Research Institute, P. O. Box 28281, San Antonio 6, Texas	1
Dr. Neidhardt, General American Transportation Corporation, 7501 N. Natches Avenue, Niles, Illinois	1
Dr. T. H. Schiffman, Armour Research Foundation, 10 West 35th St., Chicago 16, Illinois	1
Mr. Marc Peter, Jr., E. H. Plesset Associates, Inc., 2444 Wilshire Boulevard, Santa Monica, California	1
Professor M. G. Spangler, Iowa State University, Ames, Iowa	1
Mr. Sherwood Smith, Roland F. Beers, Inc., 2520 Oakville, Alexandria, Va.	1
Mr. J. Baston, Space Technology Laboratories, Inc., 5500 West El Segundo Blvd., Los Angeles 45, California	1
Dr. Frank Shelton, Kaman Nuclear, Colorado Springs, Colorado	1
Paul Weidlinger, Consulting Engineer, 770 Lexington Ave., New York 21, New York, Attn: Dr. M. Baron	1
Mr. A. Weiderman, Armour Research Foundation, 10 West 35th St., Chicago 16, Illinois	1